

Fine-Grained Image-Text Correspondence with Cost Aggregation for Open-Vocabulary Part Segmentation

Jiho Choi^{1*}, Seonho Lee^{1*}, Minhyun Lee², Seungho Lee², Hyunjung Shim^{1†}

¹KAIST, Republic of Korea

²Samsung Electronics, Republic of Korea

{jihochoi, glanceyes, kateshim}@kaist.ac.kr, {mh315.lee, sh622.lee}@samsung.com

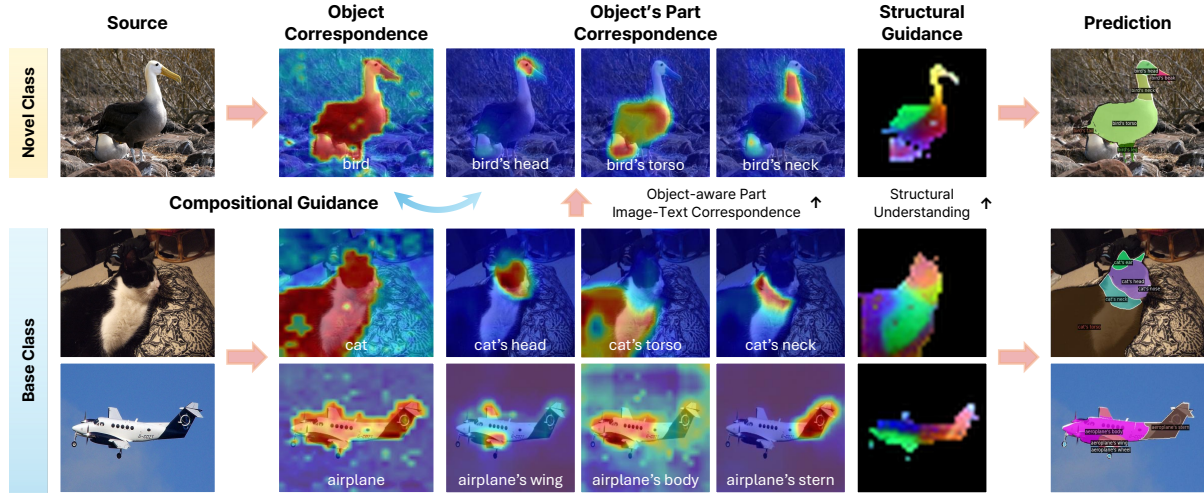


Figure 1. The proposed PartCATSeg exploits part-level and object-level image-text correspondence using cost aggregation, enhancing object-aware part image-text matching. Additionally, it utilizes structural guidance to achieve successful part segmentation even for classes not encountered during training.

Abstract

Open-Vocabulary Part Segmentation (OVPS) is an emerging field for recognizing fine-grained parts in unseen categories. We identify two primary challenges in OVPS: (1) the difficulty in aligning part-level image-text correspondence, and (2) the lack of structural understanding in segmenting object parts. To address these issues, we propose PartCATSeg, a novel framework that integrates object-aware part-level cost aggregation, compositional loss, and structural guidance from DINO. Our approach employs a disentangled cost aggregation strategy that handles object and part-level costs separately, enhancing the precision of part-level segmentation. We also introduce a compositional loss to better capture part-object relationships, compensating for the limited part annotations. Additionally, structural guidance from DINO features improves boundary delineation and inter-part understanding. Extensive experiments

on Pascal-Part-116, ADE20K-Part-234, and PartImageNet datasets demonstrate that our method significantly outperforms state-of-the-art approaches, setting a new baseline for robust generalization to unseen part categories.

1. Introduction

The rapid advancements in model architectures and improved training techniques have allowed cutting-edge models to achieve exceptional performance on closed-set datasets and object-level segmentation [6, 9, 10, 28, 36, 48, 59]. However, they still exhibit suboptimal performance in zero-shot scenarios [1, 2, 4, 20] and open-vocabulary setups [22, 40, 74, 79, 81]. Moreover, part-level fine-grained segmentation [3, 8, 25] remains challenging, highlighting the ongoing difficulties in these research areas.

Recently, Open-Vocabulary Part Segmentation (OVPS) has emerged as a novel approach aimed at recognizing novel objects at a fine-grained, part level [14, 38, 61, 70]. OVPS enables the segmentation of detailed object parts, even for

*Equal contribution

†Corresponding author

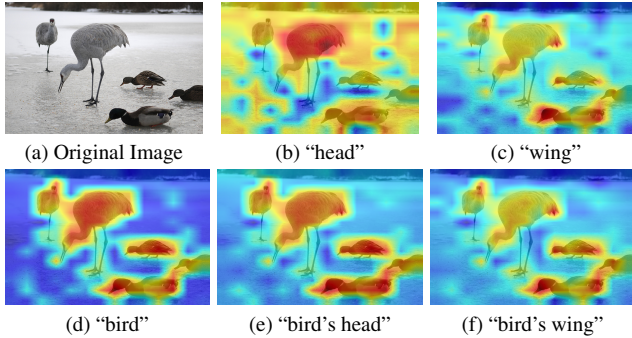


Figure 2. **CLIP Image-Text Similarity Visualization for Object-Level and Part-Level Text.** The visualization [39] compares the frozen CLIP [57] image-text similarity between object-level and part-level text descriptions. (a) shows the original images; (b), (c) depict the part-level similarities for terms such as "head" and "wing" while (e), (f) show object-specific parts. The stronger activation for object-level text in (d) suggests a dominant focus on the entire object rather than individual parts in the image-text correspondence.

categories not seen during training, positioning it as both a research challenge and a high-demand application area. This framework has numerous practical applications, including robotic control [67, 75], medical imaging [76], image editing [42, 46], and image generation [34, 69], serving as a significant milestone for the advancement of visual systems.

OVPS research has recently accelerated, leveraging pre-trained vision-language models (VLMs) [33, 37, 57] to transfer part-level knowledge from base to novel classes. Recently, VLPART [61] utilizes DINO [5, 54] features to establish part-level correspondence between base and novel categories, while OV-PARTS [70] focuses on leveraging object-level contextual information to enhance part-level segmentation. More recent approaches, such as PartGLEE [38] and PartCLIPSeg [14], further advance the field by employing attention-based approaches with joint training of object and part to refine part segmentation.

Despite recent advancements, OVPS still suffers from poor performance, as key challenges remain unresolved. First, aligning part-level text with its corresponding visual features is more challenging than at the object level. This stems from the significantly lower ratio of part-level text-image pairs compared to object-level text during the pre-training of VLMs, as noted in previous studies [25, 55, 61]. Consequently, part-level data often receives weaker or noisier guidance compared to object-level data due to its diversity. Additionally, the limited availability of part-level ground truth (GT) labels in base datasets further degrades performance. Figure 2 (b, c, e, f) illustrate the lower similarity and weaker alignment of part-level text compared to object-level text [39, 57] in pretrained CLIP.

Second, current OVPS approaches struggle to achieve a comprehensive structural understanding between parts and

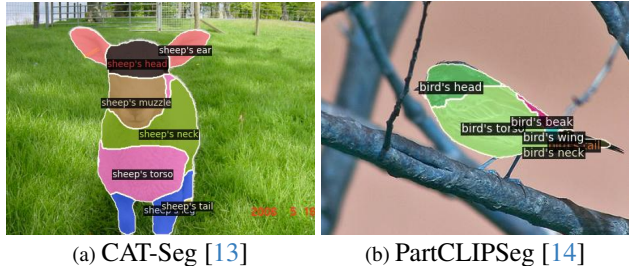


Figure 3. **Challenges of Current OVPS.** (a, b) Prediction results of state-of-the-art OVSS [13] and OVPS [14] methods. Due to a lack of structural understanding, these methods often produce incorrect OVPS predictions, such as predicting a "sheep's neck" as being larger than its "torso" or placing a "bird's beak" and a "bird's neck" at the tip of its "tail".

objects. As shown in Figure 3, existing state-of-the-art models may misclassify a "leg" as a "tail" due to an incomplete understanding of part-object relationships and structural information. This happens because the visual features of the "leg" resemble those of the "tail", leading to misrecognition. This issue is similar to the part-whole illusion [62] observed in humans when focusing only on parts without considering the whole.

We propose a novel framework, PartCATSeg, to address the critical challenges of OVPS and significantly improve model performance, as summarized in Figure 1. First, we focus on the issue of *part-level image guidance* being biased toward object-level guidance and propose a solution to mitigate this bias. Specifically, we adopt a cost aggregation strategy for explicit handling of image-text correspondence, as outlined in [11, 13]. Then, we extend this model architecture to separate and operate with cost volumes tailored to both object and part levels. This extension enables our model to disentangle and process object-level and part-level costs independently. This change provides more precise guidance and enhances image-text alignment, particularly at the part level. To further augment training signals, we integrate an unsupervised compositional loss that enforces the compositional relationship where parts collectively represent the object. This approach ensures robust part representation even with the lack of explicit part-level supervision.

Second, we leverage DINO [36, 54] features for *structural guidance* to improve the model's ability to understand inter-part relationships and effectively separate objects from the background. Previous works, such as VLPART, highlighted DINO's rich semantic representations and utilized them for matching novel classes to their closest base classes. Unlike their perspective, our study focuses on DINO's capability to convey spatial structure and geometric proximity information between features. To fully exploit this rich geometric prior, we incorporate pixel-level features as guidance when conducting the cost aggregation. This pixel-level similarity between features proves particularly beneficial for

distinguishing parts.

Our approach sets a new standard baseline for OVPS, demonstrating remarkable performance gains across diverse unseen categories in multiple datasets. Extensive experiments on benchmark datasets such as Pascal-Part-116, ADE20K-Part-234, and PartImageNet show that our method significantly outperforms existing state-of-the-art methods. We achieve notable improvements in segmentation accuracy and generalization capabilities, with increases in h-IoU scores by over 10% on all datasets in the Pred-All setting. Our analyses confirm that the combination of object-aware part-level cost aggregation techniques, the compositional loss, and structural guidance from DINO contribute to these performance gains, validating the effectiveness of our proposed framework in addressing the critical challenges of OVPS.

2. Related Work

Open-Vocabulary Semantic Segmentation (OVSS). OVSS [22, 35, 45, 50, 71, 72, 77–79, 81, 83] advances beyond traditional semantic segmentation’s [6, 10, 28] predefined class limitation by enabling predictions for unseen classes. OVSS methods generally rely on the shared embedding space of vision-language models (VLMs) [33, 37, 57] such as CLIP, allowing both visual and text features to be aligned in a unified semantic space. There are two main approaches. The first approach is a two-stage approach [18, 21, 24, 40, 45, 73, 74, 78], such as ZSSeg and ODISE, that first generates class-agnostic masks before VLM-based classification. The second approach is single-stage frameworks [13, 35, 50, 72, 77, 83] such as CLIPSeg and CAT-Seg that directly align pixel-level features with text features.

Dense Correspondence and Cost Aggregation. In computer vision, *cost* computation is used to evaluate *dense visual correspondence* [7, 11, 29–31, 44, 52, 53, 60, 63] by assessing the differences between matching points. From the perspective of Optimal Transport [56, 66], this cost reflects the difficulty of matching or high disparity. Minimizing disparity aligns with maximizing similarity. Hence, we interpret cost as a measure of correspondence, similar to prior notations [7, 11, 29, 30]. *Cost Aggregation* [7, 11, 12, 29, 31, 60, 63] is a key framework to reduce matching errors and enhance generalization in dense correspondence tasks. Early methods using handcrafted approaches [16, 43] transitioned to learnable kernels with 2D and 4D convolutions [29, 58]. With the advent of Transformer architectures, CATs and CATs++ [11, 12] demonstrated the effectiveness of Transformer-based cost aggregation. Recently, CAT-Seg [13] extended this concept to multi-modal settings, using cosine similarity between image and text embeddings as a matching cost volume. In this study, we apply cost aggregation to open-vocabulary part segmentation, en-

abling recognition of finer-grained entities.

Part Segmentation [3, 8, 8, 15, 25, 26, 32, 64] aims to recognize objects by dividing them into finer units (parts). Early works focused on contrastive and self-supervised co-part segmentation [15, 26, 32, 64], establishing foundational methods for identifying object parts without extensive labeled data. Recent developments have advanced toward open-vocabulary approaches, with notable research including VLPART [61], OV-PARTS [70], PartGLEE [38], and PartCLIPSeg [14]. VLPART aimed to generalize to novel classes using DINO correspondence [36, 54], OV-PARTS introduced object mask prompts, while PartGLEE and PartCLIPSeg combined part information with object-level context. These approaches have enhanced part segmentation performance, particularly in handling previously unseen categories. In this work, we further advance these studies by improving the image-text correspondence for both objects and parts.

3. Method

3.1. Problem Definition

Open-Vocabulary Part Segmentation (OVPS) [14, 38, 61, 70] aims to segment an image into distinct object-specific parts, $\mathbf{C}_{\text{Obj-Part}}$, (e.g., “cat’s paw,” “bus’s headlight”) without relying on predefined part categories. During training, the model uses image and ground-truth mask pairs, where the masks represent only the $\mathbf{C}_{\text{Obj-Part}}$ of base categories, $\mathbf{C}_{\text{Obj-Part}}^{\text{base}}$. At inference, the model segments novel categories, $\mathbf{C}_{\text{Obj-Part}}^{\text{novel}}$, beyond these base categories, leveraging learned representations to generalize without additional annotations. OVPS performance is assessed in two scenarios [14, 61, 70]: In **Zero-Shot** setup, the training and test categories do not overlap ($\mathbf{C}_{\text{Obj-Part}}^{\text{base}} \cap \mathbf{C}_{\text{Obj-Part}}^{\text{novel}} = \emptyset$). While in **Cross-Dataset** setting, the model evaluated on a different dataset from the training set without fine-tuning, introducing challenges from domain shifts and differences in part granularity.

3.2. Preliminary

Image-Text Cost Computation. As described in Section 2, *cost* refers to the correspondence between image-to-image or image-to-text features. CAT-Seg [13] extends the cost computation approach to effectively model image-text correspondence, showing promising performance in object-level open-vocabulary segmentation tasks [18, 22, 79]. The initial cost $\mathbb{C} \in \mathbb{R}^{(H \times W) \times |T|}$ between the i^{th} image patch and the n^{th} text token is defined as:

$$\mathbb{C}(i, n) = \frac{D^V(i) \cdot D^L(n)}{\|D^V(i)\| \|D^L(n)\|}, \quad (1)$$

where $D^V(\cdot)$ and $D^L(\cdot)$ are dense visual and language embeddings, respectively. Here, $i \in \mathbb{R}^{(H \times W)}$ is the spatial in-

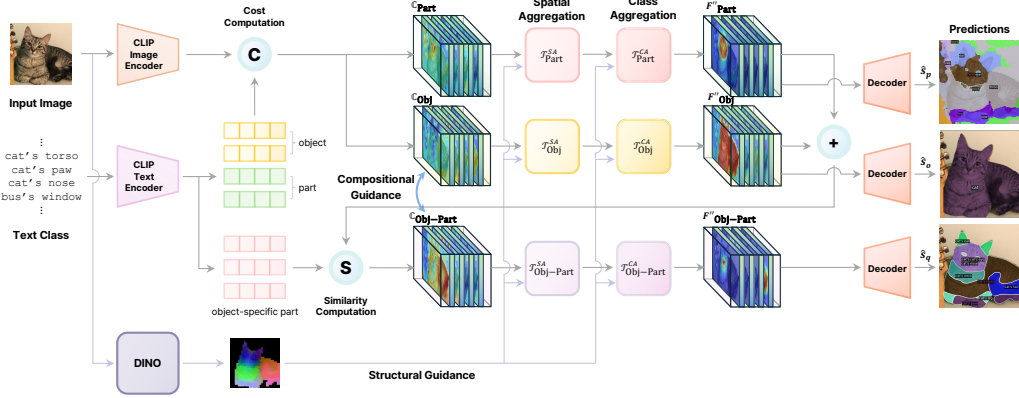


Figure 4. The Overall Architecture of PartCATSeg.

dex of the image patch and $n \in \mathbb{R}^T$ denotes the index of the text token corresponding to category classes T .

Cost Aggregation. The computed cost volume is refined through a process known as cost aggregation [7, 11, 13, 29, 30], which employs self-attention modules [65]. This process consists of two main components: the spatial aggregation transformer (\mathcal{T}^{SA}) and the class aggregation transformer (\mathcal{T}^{CA}), both of which are designed to effectively model image-text correspondence. **Spatial aggregation** utilizes the local continuity of image embeddings within the cost volume to capture spatially consistent features. Specifically, Swin Transformer [47] blocks are used to enhance semantic coherence by capturing both local and semi-global features, refining class representations, and reducing background noise. The initial cost volume feature $F \in \mathbb{R}^{(H \times W) \times |T| \times d}$ is derived from \mathbb{C} using convolutional layers, represented as: $F = \text{Conv}(\mathbb{C})$. The spatial aggregation operation for each class is then defined as:

$$F'(:, n) = \mathcal{T}^{\text{SA}}(F(:, n)), \quad F(:, n) \in \mathbb{R}^{(H \times W) \times d}, \quad (2)$$

where \mathcal{T}^{SA} is applied independently for each class in the cost volume. **Class aggregation** models inter-class relationships using a Transformer block without positional embeddings, ensuring permutation invariance. This operation accounts for the spatial context of each class and its interactions with other classes, enabling a holistic cost calculation for each class:

$$F''(i, :) = \mathcal{T}^{\text{CA}}(F'(i, :)), \quad F' \in \mathbb{R}^{(H \times W) \times |T| \times d}. \quad (3)$$

This two-stage aggregation framework refines the cost volume, enhancing prediction accuracy across diverse object categories.

3.3. Disentangled Cost Aggregation

Although CAT-Seg [13] has shown promising results in open-vocabulary semantic segmentation (OVSS), its performance is limited when it comes to fine-grained, part-level

categories. This limitation arises from the predictions being biased towards object-level categories, caused by the lack of **part-level correspondence**, as shown in Figure 2.

To address this issue, we propose a method of parsing object-level and part-level class names \mathbf{C}_{Obj} and \mathbf{C}_{Part} , computing separate cost volumes for each, similar to approaches in OVPS frameworks like PartGLEE [38] and PartCLIPSeg [14]. However, our approach differentiates itself by explicitly constructing separate cost volumes from the image-text correspondence perspective. Specifically, we compute the initial cost volumes for object-level categories and part-level categories, $\mathbb{C}_{\{\text{Obj}|\text{Part}\}} \in \mathbb{R}^{(H \times W) \times |\mathbf{C}_{\{\text{Obj}|\text{Part}\}}|}$ as follows:

$$\mathbb{C}_{\{\text{Obj}|\text{Part}\}}(i, x) = \frac{D^V(i) \cdot D^L(x)}{\|D^V(i)\| \|D^L(x)\|}, \quad x \in \{o, p\}, \quad (4)$$

where o and p are the object-level and part-level class tokens, respectively, from the categories \mathbf{C}_{Obj} and \mathbf{C}_{Part} .

We then obtain initial cost volume features $F_{\text{Obj}} \in \mathbb{R}^{(H \times W) \times |\mathbf{C}_{\text{Obj}}| \times d}$ and $F_{\text{Part}} \in \mathbb{R}^{(H \times W) \times |\mathbf{C}_{\text{Part}}| \times d}$ through convolutional layers, respectively. These features are further refined using spatial and class aggregation transformers to enhance the correspondence between image regions and class tokens. This allows us to compute cost volumes that are better aligned with the hierarchical concepts, providing more precise correspondence for both object-level and part-level class tokens. As shown in Figure 4, the features are processed through a sequence of spatial and class aggregation transformers as:

$$F''_{\text{Obj}}(i, :) = \mathcal{T}^{\text{CA}}_{\text{Obj}}(\mathcal{T}^{\text{SA}}_{\text{Obj}}(F_{\text{Obj}}(i, :))), \quad (5)$$

$$F''_{\text{Part}}(i, :) = \mathcal{T}^{\text{CA}}_{\text{Part}}(\mathcal{T}^{\text{SA}}_{\text{Part}}(F_{\text{Part}}(i, :))), \quad (6)$$

where i is a spatial location index. The refined cost volume embeddings F''_{Obj} and F''_{Part} are then fed into decoders to generate prediction masks \hat{s}_o for objects and \hat{s}_p for parts. These predictions are supervised using the corresponding

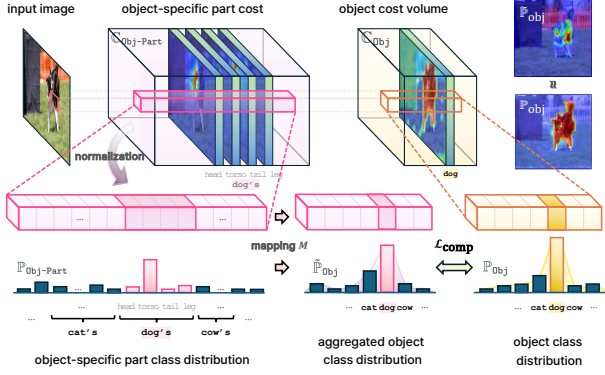


Figure 5. **Compositional Loss.** The loss function $\mathcal{L}_{\text{comp}}$ guides learning by ensuring that the aggregated class distribution of object parts aligns closely with the overall class distribution of the object, enhancing the consistency between part-level and object-level representations.

ground truth masks s_o, s_p with **disentanglement loss** as:

$$\mathcal{L}_{\text{disen}} = \lambda_{\text{obj}} \sum_{o \in \mathbf{C}_{\text{Obj}}} \text{BCE}(s_o, \hat{s}_o) + \lambda_{\text{part}} \sum_{p \in \mathbf{C}_{\text{Part}}} \text{BCE}(s_p, \hat{s}_p), \quad (7)$$

where BCE denotes the binary cross-entropy loss, and λ_{obj} and λ_{part} are hyperparameters balancing two losses. By leveraging this decoupled and disentangled cost aggregation strategy, our approach effectively enhances object-aware part-level image-text correspondence.

3.4. Object-aware Part Cost Aggregation

To further enhance image-text correspondence for object-specific parts, we integrate the object-level cost feature F_{Obj}'' and the part-level cost feature F_{Part}'' . This integration forms an object-part combination, denoted as $\mathcal{F}_{\text{Obj-Part}} \in \mathbb{R}^{(H \times W) \times |\mathbf{C}_{\text{Obj-Part}}| \times d}$, using a simple projection as follows:

$$\mathcal{F}_{\text{Obj-Part}}(i) = \text{Linear}([F_{\text{Obj}}''(i); F_{\text{Part}}''(i)]), \quad (8)$$

where $[\cdot; \cdot]$ denotes concatenation and Linear is a projection layer. By combining object and part features, the model integrates object-level context with part-level details. We then align the integrated features with the object-specific part category names, $\mathbf{C}_{\text{Obj-Part}}$, by computing the similarity between $\mathcal{F}_{\text{Obj-Part}}$ and the object-specific part text embeddings $q \in \mathbf{C}_{\text{Obj-Part}}$, thereby obtaining $\mathbf{C}_{\text{Obj-Part}}$ as:

$$\mathbf{C}_{\text{Obj-Part}}(i, q) = \frac{\mathcal{F}_{\text{Obj-Part}}(i, q) \cdot D^L(q)}{\|\mathcal{F}_{\text{Obj-Part}}(i, q)\| \|D^L(q)\|}. \quad (9)$$

The updated object-aware part cost undergoes a convolution operation to transform it into a feature representation, $F_{\text{Obj-Part}}$, before refinement through spatial and class aggregation transformers.

$$F_{\text{Obj-Part}}''(i, \cdot) = \mathcal{T}_{\text{Obj-Part}}^{\text{CA}}(\mathcal{T}_{\text{Obj-Part}}^{\text{SA}}(F_{\text{Obj-Part}}(i, \cdot))), \quad (10)$$

where $F_{\text{Obj-Part}}$ is a convoluted object-aware cost feature from $\mathbf{C}_{\text{Obj-Part}}$. By propagating object-level and part-level semantics between image and text, this approach improves image-text correspondence alignment, enhancing accurate boundary recognition at both object and part levels. Finally, the refined object-aware part embeddings $F_{\text{Obj-Part}}$ are fed into the shared decoder to generate the prediction masks \hat{s}_q and supervised using the ground truth masks s_q with the following loss: $\mathcal{L}_{\text{Obj-Part}} = \sum_{q \in \mathbf{C}_{\text{Obj-Part}}} \text{BCE}(s_q, \hat{s}_q)$.

3.5. Cost as Compositional Components

Parts are *compositional components* that constitute an object. However, the ground truth annotations for parts are relatively scarce compared to those for objects, making supervision from part annotations alone insufficient.

Compositional Bias. To address this problem, we propose a compositional loss, $\mathcal{L}_{\text{comp}}$, that enforces inductive bias of ensuring that the parts are the compositional component of its object. This loss function enhances the model’s capacity to capture spatial relationships among parts and improves the part boundary delineation, particularly for smaller components. Specifically, at each spatial location $i \in \mathbb{R}^{(H \times W)}$ in the cost volumes, we compute the normalized distributions \mathbb{P}_{Obj} and $\mathbb{P}_{\text{Obj-Part}}$ over object and part classes, respectively, by applying a softmax function to \mathbf{C}_{Obj} and $\mathbf{C}_{\text{Obj-Part}}$ along the class dimension as:

$$\mathbb{P}_{\text{Obj}}(i, o) = \frac{\exp(\mathbf{C}_{\text{Obj}}(i, o))}{\sum_{k \in \mathbf{C}_{\text{Obj}}} \exp(\mathbf{C}_{\text{Obj}}(i, k))}, \quad (11)$$

$$\mathbb{P}_{\text{Obj-Part}}(i, p) = \frac{\exp(\mathbf{C}_{\text{Obj-Part}}(i, p))}{\sum_{k \in \mathbf{C}_{\text{Obj-Part}}} \exp(\mathbf{C}_{\text{Obj-Part}}(i, k))}. \quad (12)$$

We then map the part distributions to their corresponding object classes using a predefined mapping $M : \{1, \dots, |\mathbf{C}_{\text{Obj-Part}}|\} \rightarrow \{1, \dots, |\mathbf{C}_{\text{Obj}}|\}$, which is deterministically defined based on $\mathbf{C}_{\text{Obj-Part}}$. The aggregated object class distribution $\tilde{\mathbb{P}}_{\text{Obj}} \in \mathbb{R}^{(H \times W) \times |\mathbf{C}_{\text{Obj}}|}$ is then obtained by summing the mapped part probabilities as:

$$\tilde{\mathbb{P}}_{\text{Obj}}(i, o) = \sum_{p \in M^{-1}(o)} \mathbb{P}_{\text{Obj-Part}}(i, p). \quad (13)$$

We finally compute the Jensen-Shannon [19, 41] divergence between the object’s distribution and the aggregated object distribution at each spatial location:

$$\mathcal{L}_{\text{comp}} = \frac{1}{2} \left(D_{\text{KL}}(\mathbb{P}_{\text{Obj}} \parallel \tilde{\mathbb{P}}_{\text{Obj}}) + D_{\text{KL}}(\tilde{\mathbb{P}}_{\text{Obj}} \parallel \mathbb{P}_{\text{Obj}}) \right), \quad (14)$$

By enforcing the similarity between the object’s distribution and the aggregated object distribution, we inject the inductive bias that parts collectively compose the object. This encourages the model to recognize the spatial relationships among parts and ensures that smaller parts are appropriately delineated.

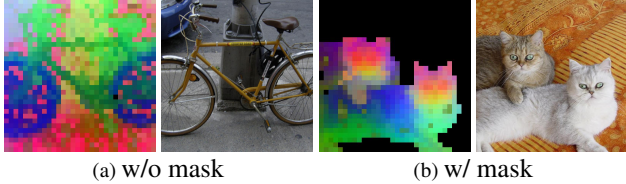


Figure 6. **Visualization of Frozen DINO PCA results.** (a) Without mask: The PCA visualization shows that DINO can separate object features from the background. (b) With mask: highlights consistent feature values across structurally similar parts of the objects, indicating strong part correspondences. This showcases DINO’s ability to capture detailed object representations.

Ultimately, our training objective aims to minimize the following loss function:

$$\mathcal{L} = \mathcal{L}_{\text{Obj-Part}} + \mathcal{L}_{\text{disen}} + \lambda_{\text{comp}} \mathcal{L}_{\text{comp}}, \quad (15)$$

where λ_{comp} is a hyperparameter for balancing the loss.

3.6. Cost with Structural Guidance

We utilize DINO’s [5, 54] self-supervised learning capabilities, which are known to exhibit strong semantic and geometric priors. DINO features have previously demonstrated their effectiveness in VLPART [61] by aiding in the correspondence computation between base and novel classes. While VLPART focused on image-to-image correspondences, we extend this approach by forming an image-text cost volume, enabling the use of DINO features for image-text correspondence directly related to specific categories.

We employ DINO features to provide structural guidance during spatial aggregation. As shown in Figure 6 (a), the PCA visualization illustrates that DINO features effectively distinguish between objects and background components. Additionally, in Figure 6 (b), after background masking and PCA application, we observed detailed intra-object information, revealing continuous PCA results within objects. This indicates that DINO features effectively capture structural information useful for predicting part relationships. The visualization further shows consistent representations for structurally similar parts (e.g., “heads” in red, “torso” in blue, and “legs” in green for two “cats”), demonstrating the alignment capability of DINO features.

Structural Guidance. To maximize the use of these structural features, we introduce structural guidance during the spatial aggregation process by incorporating it into the *Query* and *Key* matrices along with the cost volume as:

$$F'(:, n) = \mathcal{T}^{\text{SA}}(F(:, n), F_{\text{dino}}(:, n)) \in \mathbb{R}^{(H \times W) \times (d + d_{\text{dino}})}. \quad (16)$$

The effectiveness of our approach is comprehensively evaluated in the ablation study (see Section 4.3). The study demonstrates the impact of incorporating structural guidance into the cost volume, leading to improved part and object image-text correspondences.

4. Experiments

4.1. Experimental Setup

Datasets. We perform our evaluation on three OVPS benchmarks: Pascal-Part-116 [8, 70], ADE20K-Part-234 [70, 80], and PartImageNet [25]. Pascal-Part-116 is an adapted version of PascalPart [8] of OVPS, containing 8k training images and 850 test images, with 116 part classes across 17 object categories. ADE20K-Part-234, which is a more challenging and fine-grained dataset, includes 7k training images and 1k validation images with 234 part classes in 44 object categories. PartImageNet provides 16k training images and 2.9k validation images across 158 object classes from ImageNet [17], with 40 representative classes used for cross-dataset evaluation in this study. Additionally, we use PartImageNet (OOD), a split originally designed for few-shot learning, consisting of 109 training, 19 validation, and 30 test classes. This split is included for cross-dataset evaluation. Additional details of the datasets are provided in the supplementary materials.

Evaluation Metrics. To comprehensively evaluate OVPS performance, we use two protocols: (1) **Pred-All** introduced by PartCLIPSeg [14], where the model performs segmentation without access to object masks or class labels, relying entirely on its own predictions, and (2) **Oracle-Obj**, where ground truth object-level masks and class labels are provided as in setting of OV-PARTS [70]. This setup assumes the scenario of part segmentation with the reliance on an object-level segmentation results. We measure segmentation performance using mIoU and assess generalization via the harmonic mean (h-IoU) of seen and unseen categories.

Implementation Details. We adopted the training approach of CAT-Seg [13] and fine-tuned the Query and Value heads of CLIP’s encoders. Details on the information on the experimental setup, hyperparameters, and training can be found in the supplementary materials.

4.2. Main Results

Zero-Shot Part Segmentation. We compare PartCATSeg with previous methods on three popular OVPS benchmarks, demonstrating its significant performance and strong generalization capabilities. As shown in Table 1, PartCATSeg consistently outperforms existing methods on Pascal-Part-116, with significant improvements in h-IoU: a 15.10% increase in Pred-All and 11.62% increase in Oracle-Obj over the second-best method, PartCLIPSeg [14]. On the more challenging ADE20K-Part-234 dataset, as demonstrated in Table 2, PartCATSeg again outperforms previous SoTA methods, achieving a remarkable 12.81% improvement in Pred-All and 8.13% in Oracle-Obj. On PartImageNet, as in Table 3, PartCATSeg sets new performance benchmarks, breaking through the h-IoU thresholds with 55.12% in Pred-All and 72.66% in Oracle-Obj. These re-

Method	Pred-All			Oracle-Obj		
	Seen	Unseen	h-IoU	Seen	Unseen	h-IoU
ZSSeg+ [74]	38.05	3.38	6.20	54.43	19.04	28.21
VLPart [61]	35.21	9.04	14.39	42.61	18.70	25.99
CLIPSeg [50, 70]	27.79	13.27	17.96	48.91	27.54	35.24
CAT-Seg [13, 70]	36.80	23.39	28.60	43.81	27.66	33.91
PartGLEE [38]	-	-	-	<u>57.43</u>	27.41	37.11
PartCLIPSeg [14]	<u>43.91</u>	<u>23.56</u>	<u>30.67</u>	50.02	<u>31.67</u>	<u>38.79</u>
PartCATSeg (Ours)	52.62	40.51	45.77	57.49	44.88	50.41
			(+15.10)			(+11.62)

¹ The best score is **bold** and the second-best score is underlined.

Table 1. Comparison of zero-shot performance with state-of-the-art methods on Pascal-Part-116.

Method	Pred-All			Oracle-Obj		
	Seen	Unseen	h-IoU	Seen	Unseen	h-IoU
ZSSeg+ [74]	32.20	0.89	1.74	43.19	27.84	33.85
CLIPSeg [50, 70]	3.14	0.55	0.93	38.15	30.92	34.15
CAT-Seg [13, 70]	7.02	2.36	3.53	33.80	25.93	29.34
PartGLEE [38]	-	-	-	<u>51.29</u>	35.33	<u>41.83</u>
PartCLIPSeg [14]	14.15	<u>9.52</u>	<u>11.38</u>	38.37	<u>38.82</u>	38.60
PartCATSeg (Ours)	38.87	17.56	24.19	53.13	47.16	49.96
			(+12.81)			(+8.13)

Table 2. Comparison of zero-shot performance with state-of-the-art methods on ADE20K-Part-234.

Method	Pred-All			Oracle-Obj		
	Seen	Unseen	h-IoU	Seen	Unseen	h-IoU
CLIPSeg [50, 70]	32.39	12.27	17.80	53.91	37.17	44.00
CAT-Seg [13, 70]	33.58	<u>23.04</u>	<u>27.33</u>	47.34	35.14	40.33
PartCLIPSeg [14]	<u>38.82</u>	19.47	25.94	<u>56.26</u>	<u>51.65</u>	<u>53.85</u>
PartCATSeg (Ours)	57.33	53.07	55.12	73.83	71.52	72.66
			(+27.79)			(+18.81)

Table 3. Comparison of zero-shot performance with state-of-the-art methods on PartImageNet.

sults highlight PartCATSeg’s advanced capabilities, particularly in performance on unseen categories, positioning it as a leading solution in OVPS with exceptional accuracy in both seen and unseen classes. By addressing the challenges in OVPS, our method achieves a significant advancement in OVPS, highlighting PartCATSeg’s robustness and superior generalization abilities across diverse datasets.

Cross-Dataset Part Segmentation. Our experiments evaluate the performance of our method in two cross-dataset settings: (1) PartImageNet (OOD) and (2) PartImageNet \rightarrow Pascal-Part-116. PartImageNet (OOD) includes classes with complex, irregular part shapes that differ from the training data, for evaluating adaptability to novel configurations within a familiar structure. As shown in Table 4, PartCATSeg outperforms previous methods in both Pred-All and Oracle-Obj settings, demonstrating its robustness in handling unseen categories in an OOD context. On PartImageNet \rightarrow Pascal-Part-116, we evaluate the model’s ability to transfer to a different dataset, Pascal-Part-116 [8, 70]. Trained on PartImageNet, our model is evaluated on Pascal-Part-116. Herein, PartCATSeg again achieves the highest performance across both Pred-All and Oracle-Obj settings. These results confirm PartCATSeg’s effectiveness in diverse cross-dataset scenarios, highlighting its versatility and robustness in part segmentation tasks across various dataset configurations.

Qualitative Evaluation. We present qualitative results on the

Method	PartImageNet (OOD)		PartImageNet \rightarrow Pascal-Part-116	
	Pred-All	Oracle-Obj	Pred-All	Oracle-Obj
	Unseen	Unseen	Unseen	Unseen
CLIPSeg [50, 70]	6.69	55.86	11.72	14.87
CAT-Seg [13, 70]	<u>19.83</u>	39.12	11.55	12.50
PartCLIPSeg [14]	10.33	<u>59.16</u>	<u>14.74</u>	<u>19.86</u>
PartCATSeg (Ours)	40.17	66.15	18.21	22.88
	(+20.34)	(+6.99)	(+3.47)	(+3.02)

Table 4. Cross-dataset performance with PartImageNet (OOD) and PartImageNet to Pascal-Part-116.

Compositional Loss	Pred-All			Oracle-Obj		
	Seen	Unseen	h-IoU	Seen	Unseen	h-IoU
Cost Agg	44.05	25.06	31.94	56.40	28.26	37.66
+ DINO	54.48	35.89	43.28	60.56	40.51	48.55
+ DINO + $\mathcal{L}_{\text{comp-L1}}$	54.70	<u>35.92</u>	<u>43.36</u>	61.29	<u>41.62</u>	<u>49.57</u>
+ DINO + $\mathcal{L}_{\text{comp-SM}}$	<u>52.62</u>	40.51	45.77	<u>57.49</u>	44.88	50.41

Table 5. Impact of Compositional Loss on Pascal-Part-116

Structural Guidance	Pred-All			Oracle-Obj		
	Seen	Unseen	h-IoU	Seen	Unseen	h-IoU
w/o Structural Guidance	42.29	27.94	33.65	46.44	31.59	37.60
DINO ($\mathcal{T}_{\text{Obj}}^{\text{SA}}$)	50.24	31.35	38.61	55.03	34.29	42.25
DINO ($\mathcal{T}_{\text{Part}}^{\text{SA}}$)	56.28	<u>36.67</u>	<u>44.41</u>	62.73	<u>43.47</u>	51.35
DINO ($\mathcal{T}_{\text{Obj}}^{\text{SA}}, \mathcal{T}_{\text{Part}}^{\text{SA}}$)	<u>52.62</u>	40.51	45.77	<u>57.49</u>	44.88	<u>50.41</u>

¹ All configurations use the compositional loss $\mathcal{L}_{\text{comp}}$.

² Configurations utilizing DINO also include object-specific part-level guidance.

Table 6. Impact of Structural Guidance on Pascal-Part-116.

Pascal-Part-116 dataset in the Pred-All setting. Figure 7 compares our method with other baselines, demonstrating significant improvements by addressing several challenges in previous OVPS methods. For instance, in **rows 1 and 2**, compared to the other baselines showing unnatural segmentations, our model successfully segments the cat’s leg and the dog’s neck, preserving the object’s structural integrity with the structural guidance. In **row 6**, PartCATSeg correctly segments the person’s upper and lower arm as distinct parts. Additionally, our method almost completely segments the parts in the object without leaving regions unsegmented and effectively captures smaller parts that other models often miss. For example, in **rows 2 – 4**, finer details like the dog’s ear, the cow’s tail, and the bird’s beak are accurately segmented in our method. In **rows 5 and 6**, our method segments almost all the parts in the object without sacrificing accuracy compared to the other baselines. This improvement is largely due to the compositional loss, which encourages the competitive assignment of parts that collectively constitute the whole object. Moreover, our method resolves confusion between similar object categories. In **rows 1 and 2**, other models misclassify parts of the cat and dog, sometimes confusing the cat for a dog and vice versa. Our object-aware part-level guidance helps the model correctly segment the parts of the correct object.

4.3. Ablation Study

Impact of Compositional Loss. To assess the effectiveness of the proposed compositional loss $\mathcal{L}_{\text{comp}}$, we conduct an ablation study on its impact on Pascal-Part-116 in Table 5. We compare the effects of using compositional loss with a softmax-based normal-

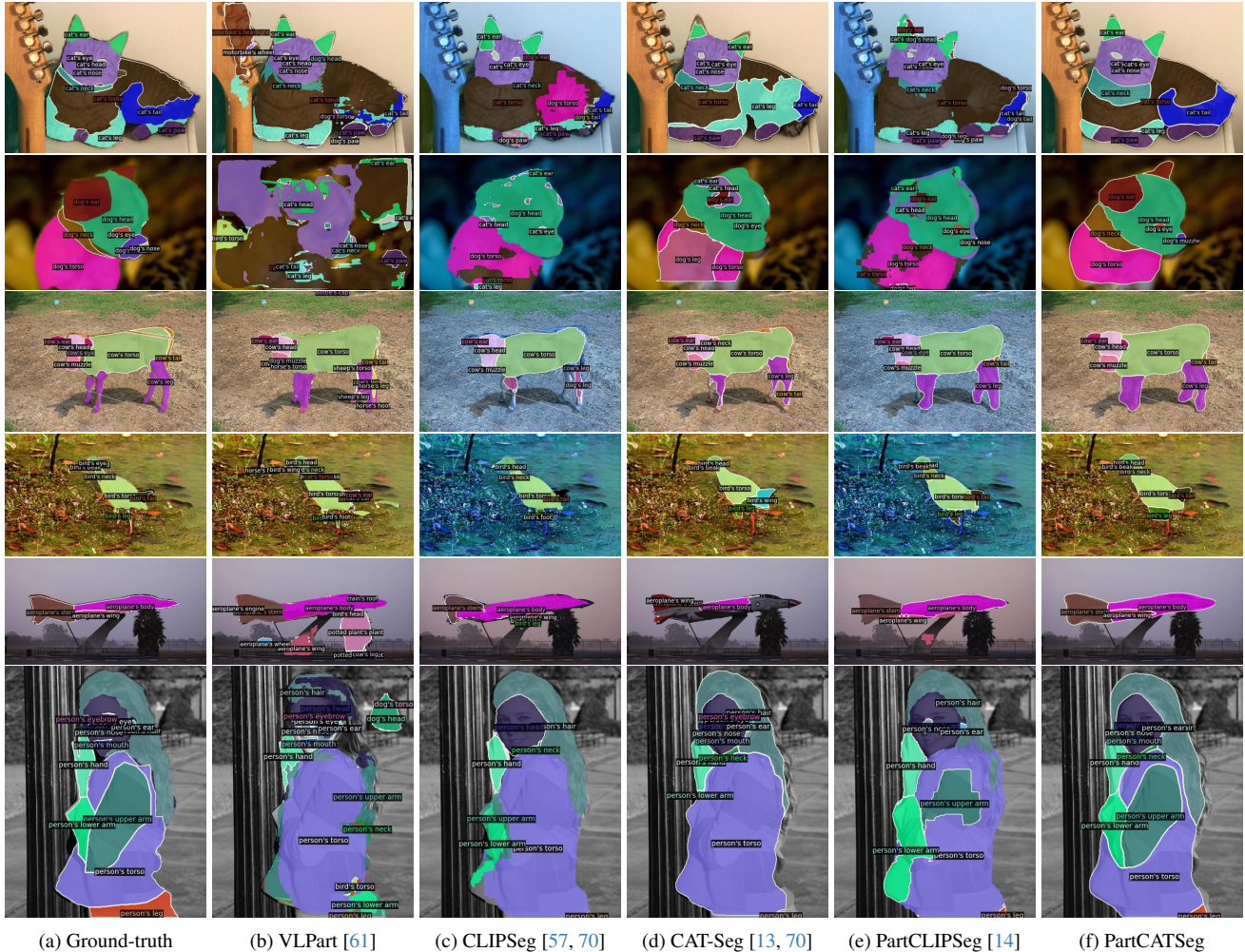


Figure 7. Qualitative evaluation of zero-shot part segmentation on Pascal-Part-116 in the **Pred-All** configuration. Note that annotations for unseen categories (e.g., bird, cow, dog) are excluded from the training set.

ization ($\mathcal{L}_{\text{comp-SM}}$), which encourages each spatial location to be predominantly assigned to a single part class, versus L1 normalization ($\mathcal{L}_{\text{comp-L1}}$) before combining part costs. We observe that adding $\mathcal{L}_{\text{comp}}$ gains about 2% h-IoU increase in the Pred-All setting compared to the model without using $\mathcal{L}_{\text{comp}}$. Furthermore, the model using $\mathcal{L}_{\text{comp-SM}}$ outperforms the one using $\mathcal{L}_{\text{comp-L1}}$. These results confirm that $\mathcal{L}_{\text{comp}}$ effectively improves performance by leveraging the inductive bias that parts collectively compose the object. Further qualitative results of ablation on $\mathcal{L}_{\text{comp}}$ are provided in the supplementary materials.

Impact of Structural Guidance from DINO. To investigate the effect of structural guidance from DINO, we conduct an ablation study by selectively applying it in our cost aggregation framework. In PartCATSeg, structural guidance from DINO is incorporated into three levels of spatial aggregation transformer modules: objects ($\mathcal{T}_{\text{Obj}}^{\text{SA}}$), parts ($\mathcal{T}_{\text{Part}}^{\text{SA}}$), and object-specific parts ($\mathcal{T}_{\text{Obj-Part}}^{\text{SA}}$). We measure performance changes on Pascal-Part-116 when structural guidance is applied only at the object level, only at the part level, and at both levels. As shown in Table 6, applying structural guidance at the part level yields more h-IoU increases in both

Pred-All and Oracle-Obj settings than at the object level. When structural guidance is applied at both levels, we observe further improvements, especially in unseen classes. This suggests that, within the cost aggregation framework, structural guidance from DINO is more effective when leveraging detailed structural information within individual objects, rather than relying solely on DINO’s background-object separation ability.

5. Conclusion

In this paper, we present a novel approach to open-vocabulary part segmentation, PartCATSeg, which leverages cost aggregation to address the inherent challenges of OVPS. We make strategic modifications to cost aggregation to enhance object-aware part-level guidance, incorporate a compositional loss to compensate for limited part-level guidance from the base set, and utilize DINO features for robust structural guidance. These combined efforts enable PartCATSeg to significantly outperform existing state-of-the-art methods. We believe that our approach can serve as a powerful new baseline for practitioners and researchers, fostering greater interest and advancement within the community.

Bibliography

- [1] Zeynep Akata, Florent Perronnin, Zaid Harchaoui, and Cordelia Schmid. Label-embedding for image classification. *IEEE transactions on pattern analysis and machine intelligence*, 38(7):1425–1438, 2015. 1
- [2] Zeynep Akata, Scott Reed, Daniel Walter, Honglak Lee, and Bernt Schiele. Evaluation of output embeddings for fine-grained image classification. In *Proceedings of the IEEE conference on computer vision and pattern recognition*, pages 2927–2936, 2015. 1
- [3] Juan Antonio Balbuena, Raúl Míguez-Lozano, and Isabel Blasco-Costa. Paco: a novel procrustes application to co-phylogenetic analysis. *PLoS one*, 8(4):e61048, 2013. 1, 3
- [4] Maxime Bucher, Tuan-Hung Vu, Matthieu Cord, and Patrick Pérez. Zero-shot semantic segmentation. *Advances in Neural Information Processing Systems*, 32, 2019. 1
- [5] Mathilde Caron, Hugo Touvron, Ishan Misra, Hervé Jégou, Julien Mairal, Piotr Bojanowski, and Armand Joulin. Emerging properties in self-supervised vision transformers. In *Proceedings of the IEEE/CVF international conference on computer vision*, pages 9650–9660, 2021. 2, 6
- [6] Liang-Chieh Chen. Rethinking atrous convolution for semantic image segmentation. *arXiv preprint arXiv:1706.05587*, 2017. 1, 3
- [7] Weitao Chen, Hongbin Xu, Zhipeng Zhou, Yang Liu, Baigui Sun, Wenxiong Kang, and Xuansong Xie. Costformer: Cost transformer for cost aggregation in multi-view stereo. *arXiv preprint arXiv:2305.10320*, 2023. 3, 4
- [8] Xianjie Chen, Roozbeh Mottaghi, Xiaobai Liu, Sanja Fidler, Raquel Urtasun, and Alan Yuille. Detect what you can: Detecting and representing objects using holistic models and body parts. In *Proceedings of the IEEE conference on computer vision and pattern recognition*, pages 1971–1978, 2014. 1, 3, 6, 7, 5
- [9] Bowen Cheng, Alex Schwing, and Alexander Kirillov. Pixel classification is not all you need for semantic segmentation. *Advances in neural information processing systems*, 34:17864–17875, 2021. 1
- [10] Bowen Cheng, Ishan Misra, Alexander G Schwing, Alexander Kirillov, and Rohit Girdhar. Masked-attention mask transformer for universal image segmentation. In *Proceedings of the IEEE/CVF conference on computer vision and pattern recognition*, pages 1290–1299, 2022. 1, 3
- [11] Seokju Cho, Sunghwan Hong, Sangryul Jeon, Yunsung Lee, Kwanghoon Sohn, and Seungryong Kim. Cats: Cost aggregation transformers for visual correspondence. *Advances in Neural Information Processing Systems*, 34:9011–9023, 2021. 2, 3, 4
- [12] Seokju Cho, Sunghwan Hong, and Seungryong Kim. Cats++: Boosting cost aggregation with convolutions and transformers. *IEEE Transactions on Pattern Analysis and Machine Intelligence*, 45(6):7174–7194, 2022. 3
- [13] Seokju Cho, Heeseong Shin, Sunghwan Hong, Seungjun An, Seungjun Lee, Anurag Arnab, Paul Hongsuck Seo, and Seungryong Kim. Cat-seg: Cost aggregation for open-vocabulary semantic segmentation. *arXiv preprint arXiv:2303.11797*, 2023. 2, 3, 4, 6, 7, 8, 1, 9, 10
- [14] Jiho Choi, Seonho Lee, Seungho Lee, Minhyun Lee, and Hyunjung Shim. Understanding multi-granularity for open-vocabulary part segmentation. *arXiv preprint arXiv:2406.11384*, 2024. 1, 2, 3, 4, 6, 7, 8, 9, 10
- [15] Subhabrata Choudhury, Iro Laina, Christian Rupprecht, and Andrea Vedaldi. Unsupervised part discovery from contrastive reconstruction. *Advances in Neural Information Processing Systems*, 34:28104–28118, 2021. 3
- [16] Navneet Dalal and Bill Triggs. Histograms of oriented gradients for human detection. In *2005 IEEE computer society conference on computer vision and pattern recognition (CVPR’05)*, pages 886–893. Ieee, 2005. 3
- [17] Jia Deng, Wei Dong, Richard Socher, Li-Jia Li, Kai Li, and Li Fei-Fei. Imagenet: A large-scale hierarchical image database. In *2009 IEEE conference on computer vision and pattern recognition*, pages 248–255. Ieee, 2009. 6
- [18] Zheng Ding, Jieke Wang, and Zhuowen Tu. Open-vocabulary universal image segmentation with maskclip. *arXiv preprint arXiv:2208.08984*, 2022. 3
- [19] Erik Englesson and Hossein Azizpour. Generalized jensen-shannon divergence loss for learning with noisy labels. *Advances in Neural Information Processing Systems*, 34:30284–30297, 2021. 5
- [20] Andrea Frome, Greg S Corrado, Jon Shlens, Samy Bengio, Jeff Dean, Marc’Aurelio Ranzato, and Tomas Mikolov. Devise: A deep visual-semantic embedding model. *Advances in neural information processing systems*, 26, 2013. 1
- [21] Golnaz Ghiasi, Xiuye Gu, Yin Cui, and Tsung-Yi Lin. Scaling open-vocabulary image segmentation with image-level labels. In *European Conference on Computer Vision*, pages 540–557. Springer, 2022. 3
- [22] Xiuye Gu, Tsung-Yi Lin, Weicheng Kuo, and Yin Cui. Open-vocabulary object detection via vision and language knowledge distillation. *arXiv preprint arXiv:2104.13921*, 2021. 1, 3
- [23] Tae Jun Ham, Sung Jun Jung, Seonghak Kim, Young H Oh, Yeonhong Park, Yoonho Song, Jung-Hun Park, Sanghee Lee, Kyoung Park, Jae W Lee, et al. A³: Accelerating attention mechanisms in neural networks with approximation. In *2020 IEEE International Symposium on High Performance Computer Architecture (HPCA)*, pages 328–341. IEEE, 2020. 1
- [24] Kunyang Han, Yong Liu, Jun Hao Liew, Henghui Ding, Jiajun Liu, Yitong Wang, Yansong Tang, Yujia Yang, Jiashi Feng, Yao Zhao, et al. Global knowledge calibration for fast open-vocabulary segmentation. In *Proceedings of the IEEE/CVF International Conference on Computer Vision*, pages 797–807, 2023. 3
- [25] Ju He, Shuo Yang, Shaokang Yang, Adam Kortylewski, Xiaoding Yuan, Jie-Neng Chen, Shuai Liu, Cheng Yang, Qihang Yu, and Alan Yuille. Partimagenet: A large, high-quality dataset of parts. In *European Conference on Computer Vision*, pages 128–145. Springer, 2022. 1, 2, 3, 6, 7
- [26] Ju He, Jieneng Chen, Ming-Xian Lin, Qihang Yu, and Alan L Yuille. Composer: Bottom-up clustering and compositing for robust part and object segmentation. In *Proceedings of the IEEE/CVF Conference on Computer Vision and Pattern Recognition*, pages 11259–11268, 2023. 3

- [27] Kaiming He, Xiangyu Zhang, Shaoqing Ren, and Jian Sun. Deep residual learning for image recognition. In *Proceedings of the IEEE conference on computer vision and pattern recognition*, pages 770–778, 2016. 2
- [28] Kaiming He, Georgia Gkioxari, Piotr Dollár, and Ross Girshick. Mask r-cnn. In *Proceedings of the IEEE international conference on computer vision*, pages 2961–2969, 2017. 1, 3
- [29] Sunghwan Hong, Seokju Cho, Jisu Nam, Stephen Lin, and Seungryong Kim. Cost aggregation with 4d convolutional swin transformer for few-shot segmentation. In *European Conference on Computer Vision*, pages 108–126. Springer, 2022. 3, 4
- [30] Sunghwan Hong, Seokju Cho, Seungryong Kim, and Stephen Lin. Unifying feature and cost aggregation with transformers for semantic and visual correspondence. In *The Twelfth International Conference on Learning Representations*, 2024. 3, 4
- [31] Asmaa Hosni, Christoph Rhemann, Michael Bleyer, Carsten Rother, and Margrit Gelautz. Fast cost-volume filtering for visual correspondence and beyond. *IEEE transactions on pattern analysis and machine intelligence*, 35(2):504–511, 2012. 3
- [32] Wei-Chih Hung, Varun Jampani, Sifei Liu, Pavlo Molchanov, Ming-Hsuan Yang, and Jan Kautz. Scops: Self-supervised co-part segmentation. In *Proceedings of the IEEE/CVF Conference on Computer Vision and Pattern Recognition*, pages 869–878, 2019. 3
- [33] Chao Jia, Yinfei Yang, Ye Xia, Yi-Ting Chen, Zarana Parekh, Hieu Pham, Quoc Le, Yun-Hsuan Sung, Zhen Li, and Tom Duerig. Scaling up visual and vision-language representation learning with noisy text supervision. In *International conference on machine learning*, pages 4904–4916. PMLR, 2021. 2, 3
- [34] Juil Koo, Seungwoo Yoo, Minh Hieu Nguyen, and Minhyuk Sung. Salad: Part-level latent diffusion for 3d shape generation and manipulation. In *Proceedings of the IEEE/CVF International Conference on Computer Vision*, pages 14441–14451, 2023. 2
- [35] Boyi Li, Kilian Q Weinberger, Serge Belongie, Vladlen Koltun, and René Ranftl. Language-driven semantic segmentation. *arXiv preprint arXiv:2201.03546*, 2022. 3
- [36] Feng Li, Hao Zhang, Huaizhe Xu, Shilong Liu, Lei Zhang, Lionel M Ni, and Heung-Yeung Shum. Mask dino: Towards a unified transformer-based framework for object detection and segmentation. In *Proceedings of the IEEE/CVF Conference on Computer Vision and Pattern Recognition*, pages 3041–3050, 2023. 1, 2, 3
- [37] Junnan Li, Dongxu Li, Caiming Xiong, and Steven Hoi. Blip: Bootstrapping language-image pre-training for unified vision-language understanding and generation. In *International conference on machine learning*, pages 12888–12900. PMLR, 2022. 2, 3
- [38] Junyi Li, Junfeng Wu, Weizhi Zhao, Song Bai, and Xiang Bai. Partglee: A foundation model for recognizing and parsing any objects. *arXiv preprint arXiv:2407.16696*, 2024. 1, 2, 3, 4, 7
- [39] Yi Li, Hualiang Wang, Yiqun Duan, and Xiaomeng Li. Clip surgery for better explainability with enhancement in open-vocabulary tasks. *arXiv preprint arXiv:2304.05653*, 2023. 2
- [40] Feng Liang, Bichen Wu, Xiaoliang Dai, Kunpeng Li, Yanan Zhao, Hang Zhang, Peizhao Zhang, Peter Vajda, and Diana Marculescu. Open-vocabulary semantic segmentation with mask-adapted clip. In *Proceedings of the IEEE/CVF Conference on Computer Vision and Pattern Recognition*, pages 7061–7070, 2023. 1, 3
- [41] Jianhua Lin. Divergence measures based on the shannon entropy. *IEEE Transactions on Information theory*, 37(1):145–151, 1991. 5
- [42] Huan Ling, Karsten Kreis, Daiqing Li, Seung Wook Kim, Antonio Torralba, and Sanja Fidler. Editgan: High-precision semantic image editing. *Advances in Neural Information Processing Systems*, 34:16331–16345, 2021. 2
- [43] Ce Liu, Jenny Yuen, and Antonio Torralba. Sift flow: Dense correspondence across scenes and its applications. *IEEE transactions on pattern analysis and machine intelligence*, 33(5):978–994, 2010. 3
- [44] Yanbin Liu, Linchao Zhu, Makoto Yamada, and Yi Yang. Semantic correspondence as an optimal transport problem. In *Proceedings of the IEEE/CVF Conference on Computer Vision and Pattern Recognition*, pages 4463–4472, 2020. 3
- [45] Yong Liu, Sule Bai, Guanbin Li, Yitong Wang, and Yansong Tang. Open-vocabulary segmentation with semantic-assisted calibration. *arXiv preprint arXiv:2312.04089*, 2023. 3
- [46] Zongdai Liu, Feixiang Lu, Peng Wang, Hui Miao, Liangjun Zhang, Ruigang Yang, and Bin Zhou. 3d part guided image editing for fine-grained object understanding. In *Proceedings of the IEEE/CVF Conference on Computer Vision and Pattern Recognition*, pages 11336–11345, 2020. 2
- [47] Ze Liu, Yutong Lin, Yue Cao, Han Hu, Yixuan Wei, Zheng Zhang, Stephen Lin, and Baining Guo. Swin transformer: Hierarchical vision transformer using shifted windows. In *Proceedings of the IEEE/CVF international conference on computer vision*, pages 10012–10022, 2021. 4, 1
- [48] Jonathan Long, Evan Shelhamer, and Trevor Darrell. Fully convolutional networks for semantic segmentation. In *Proceedings of the IEEE conference on computer vision and pattern recognition*, pages 3431–3440, 2015. 1
- [49] I Loshchilov. Decoupled weight decay regularization. *arXiv preprint arXiv:1711.05101*, 2017. 2
- [50] Timo Lüddecke and Alexander Ecker. Image segmentation using text and image prompts. In *Proceedings of the IEEE/CVF conference on computer vision and pattern recognition*, pages 7086–7096, 2022. 3, 7, 2
- [51] George A Miller. Wordnet: a lexical database for english. *Communications of the ACM*, 38(11):39–41, 1995. 6
- [52] Juhong Min, Jongmin Lee, Jean Ponce, and Minsu Cho. Hyperpixel flow: Semantic correspondence with multi-layer neural features. In *Proceedings of the IEEE/CVF International Conference on Computer Vision*, pages 3395–3404, 2019. 3
- [53] Juhong Min, Jongmin Lee, Jean Ponce, and Minsu Cho. Learning to compose hypercolumns for visual correspondence. In *Computer Vision—ECCV 2020: 16th European*

- Conference, Glasgow, UK, August 23–28, 2020, Proceedings, Part XV 16*, pages 346–363. Springer, 2020. 3
- [54] Maxime Oquab, Timothée Darcet, Théo Moutakanni, Huy Vo, Marc Szafraniec, Vasil Khalidov, Pierre Fernandez, Daniel Haziza, Francisco Massa, Alaaeldin El-Nouby, et al. Dinov2: Learning robust visual features without supervision. *arXiv preprint arXiv:2304.07193*, 2023. 2, 3, 6, 1
- [55] Tai-Yu Pan, Qing Liu, Wei-Lun Chao, and Brian Price. Towards open-world segmentation of parts. In *Proceedings of the IEEE/CVF Conference on Computer Vision and Pattern Recognition*, pages 15392–15401, 2023. 2
- [56] Gabriel Peyré, Marco Cuturi, et al. Computational optimal transport: With applications to data science. *Foundations and Trends® in Machine Learning*, 11(5-6):355–607, 2019. 3
- [57] Alec Radford, Jong Wook Kim, Chris Hallacy, Aditya Ramesh, Gabriel Goh, Sandhini Agarwal, Girish Sastry, Amanda Askell, Pamela Mishkin, Jack Clark, et al. Learning transferable visual models from natural language supervision. In *International conference on machine learning*, pages 8748–8763. PMLR, 2021. 2, 3, 8, 1, 9, 10
- [58] Ignacio Rocco, Mircea Cimpoi, Relja Arandjelović, Akihiko Torii, Tomas Pajdla, and Josef Sivic. Neighbourhood consensus networks. *Advances in neural information processing systems*, 31, 2018. 3
- [59] Olaf Ronneberger, Philipp Fischer, and Thomas Brox. U-net: Convolutional networks for biomedical image segmentation. In *Medical image computing and computer-assisted intervention—MICCAI 2015: 18th international conference, Munich, Germany, October 5-9, 2015, proceedings, part III 18*, pages 234–241. Springer, 2015. 1
- [60] Deqing Sun, Xiaodong Yang, Ming-Yu Liu, and Jan Kautz. Pwc-net: Cnns for optical flow using pyramid, warping, and cost volume. In *Proceedings of the IEEE conference on computer vision and pattern recognition*, pages 8934–8943, 2018. 3
- [61] Peize Sun, Shoufa Chen, Chenchen Zhu, Fanyi Xiao, Ping Luo, Saining Xie, and Zhicheng Yan. Going denser with open-vocabulary part segmentation. In *Proceedings of the IEEE/CVF International Conference on Computer Vision*, pages 15453–15465, 2023. 1, 2, 3, 6, 7, 8
- [62] James W Tanaka and Martha J Farah. Parts and wholes in face recognition. *The Quarterly Journal of Experimental Psychology Section A*, 46(2):225–245, 1993. 2
- [63] Prune Truong, Martin Danelljan, and Radu Timofte. Glunet: Global-local universal network for dense flow and correspondences. In *Proceedings of the IEEE/CVF conference on computer vision and pattern recognition*, pages 6258–6268, 2020. 3
- [64] Robert van der Klis, Stephan Alaniz, Massimiliano Mancini, Cassio F Dantas, Dino Ienco, Zeynep Akata, and Diego Marcos. Pdisconet: Semantically consistent part discovery for fine-grained recognition. In *Proceedings of the IEEE/CVF International Conference on Computer Vision*, pages 1866–1876, 2023. 3
- [65] Ashish Vaswani, Noam Shazeer, Niki Parmar, Jakob Uszkoreit, Llion Jones, Aidan N Gomez, Łukasz Kaiser, and Illia Polosukhin. Attention is all you need. *Advances in neural information processing systems*, 30, 2017. 4
- [66] Cédric Villani et al. *Optimal transport: old and new*. Springer, 2009. 3
- [67] Zifu Wan, Yaqi Xie, Ce Zhang, Zhiqiu Lin, Zihan Wang, Simon Stepputtis, Deva Ramanan, and Katia P Sycara. Instructpart: Affordance-based part segmentation from language instruction. In *AAAI-2024 Workshop on Public Sector LLMs: Algorithmic and Sociotechnical Design*, 2024. 2
- [68] Wenhai Wang, Enze Xie, Xiang Li, Deng-Ping Fan, Kaitao Song, Ding Liang, Tong Lu, Ping Luo, and Ling Shao. Pyramid vision transformer: A versatile backbone for dense prediction without convolutions. In *Proceedings of the IEEE/CVF international conference on computer vision*, pages 568–578, 2021. 1
- [69] Xudong Wang, Trevor Darrell, Sai Saketh Rambhatla, Rohit Girdhar, and Ishan Misra. Instancediffusion: Instance-level control for image generation. *arXiv preprint arXiv:2402.03290*, 2024. 2
- [70] Meng Wei, Xiaoyu Yue, Wenwei Zhang, Shu Kong, Xihui Liu, and Jiangmiao Pang. Ov-parts: Towards open-vocabulary part segmentation. *Advances in Neural Information Processing Systems*, 36, 2024. 1, 2, 3, 6, 7, 8, 5, 9, 10
- [71] Yongqin Xian, Subhabrata Choudhury, Yang He, Bernt Schiele, and Zeynep Akata. Semantic projection network for zero-and few-label semantic segmentation. In *Proceedings of the IEEE/CVF Conference on Computer Vision and Pattern Recognition*, pages 8256–8265, 2019. 3
- [72] Bin Xie, Jiale Cao, Jin Xie, Fahad Shahbaz Khan, and Yanwei Pang. Sed: A simple encoder-decoder for open-vocabulary semantic segmentation. *arXiv preprint arXiv:2311.15537*, 2023. 3
- [73] Jiarui Xu, Sifei Liu, Arash Vahdat, Wonmin Byeon, Xiaolong Wang, and Shalini De Mello. Open-vocabulary panoptic segmentation with text-to-image diffusion models. In *Proceedings of the IEEE/CVF Conference on Computer Vision and Pattern Recognition*, pages 2955–2966, 2023. 3
- [74] Mengde Xu, Zheng Zhang, Fangyun Wei, Yutong Lin, Yue Cao, Han Hu, and Xiang Bai. A simple baseline for open-vocabulary semantic segmentation with pre-trained vision-language model. In *European Conference on Computer Vision*, pages 736–753. Springer, 2022. 1, 3, 7, 2
- [75] Sriram Yenamandra, Arun Ramachandran, Karmesh Yadav, Austin Wang, Mukul Khanna, Theophile Gervet, Tsung-Yen Yang, Vidhi Jain, Alexander William Clegg, John Turner, et al. Homerobot: Open-vocabulary mobile manipulation. *arXiv preprint arXiv:2306.11565*, 2023. 2
- [76] Qihang Yu, Dong Yang, Holger Roth, Yutong Bai, Yixiao Zhang, Alan L Yuille, and Daguang Xu. C2fnas: Coarse-to-fine neural architecture search for 3d medical image segmentation. In *Proceedings of the IEEE/CVF Conference on Computer Vision and Pattern Recognition*, pages 4126–4135, 2020. 2
- [77] Qihang Yu, Ju He, Xueqing Deng, Xiaohui Shen, and Liang-Chieh Chen. Convolutions die hard: Open-vocabulary segmentation with single frozen convolutional clip. *Advances in Neural Information Processing Systems*, 36, 2024. 3
- [78] Alireza Zareian, Kevin Dela Rosa, Derek Hao Hu, and Shih-Fu Chang. Open-vocabulary object detection using captions.

- In *Proceedings of the IEEE/CVF Conference on Computer Vision and Pattern Recognition*, pages 14393–14402, 2021. [3](#)
- [79] Hang Zhao, Xavier Puig, Bolei Zhou, Sanja Fidler, and Antonio Torralba. Open vocabulary scene parsing. In *Proceedings of the IEEE International Conference on Computer Vision*, pages 2002–2010, 2017. [1](#), [3](#)
- [80] Bolei Zhou, Hang Zhao, Xavier Puig, Sanja Fidler, Adela Barriuso, and Antonio Torralba. Scene parsing through ade20k dataset. In *Proceedings of the IEEE conference on computer vision and pattern recognition*, pages 633–641, 2017. [6](#), [5](#)
- [81] Chong Zhou, Chen Change Loy, and Bo Dai. Extract free dense labels from clip. In *European Conference on Computer Vision*, pages 696–712. Springer, 2022. [1](#), [3](#)
- [82] Kaiyang Zhou, Jingkang Yang, Chen Change Loy, and Ziwei Liu. Learning to prompt for vision-language models. *International Journal of Computer Vision*, 130(9):2337–2348, 2022. [2](#)
- [83] Ziqin Zhou, Yinjie Lei, Bowen Zhang, Lingqiao Liu, and Yifan Liu. Zegclip: Towards adapting clip for zero-shot semantic segmentation. In *Proceedings of the IEEE/CVF Conference on Computer Vision and Pattern Recognition*, pages 11175–11185, 2023. [3](#)

Fine-Grained Image-Text Correspondence with Cost Aggregation for Open-Vocabulary Part Segmentation

Supplementary Material

Contents

A Limitations & Future Work	1
B Experimental Details	1
B.1. Code & Reproduction	1
B.2. Device Information	1
B.3. Implementation Details	1
B.4. Evaluation Details	2
B.5. Hyperparameters	2
B.6. Baselines	2
C Additional Quantitative Evaluation	2
C.1. Evaluation on Recall	2
C.2. DINO Structural Guidance	2
D Additional Qualitative Results	3
D.1. Pascal-Part-116 (Oracle-Obj Setting)	3
D.2. PartImageNet (Pred-All Setting)	3
D.3. PartImageNet (Oracle-Obj Setting)	3
D.4. Cost Visualization	3
E Additional Ablation Study	4
E.1. Compositional Loss	4
F. Datasets Details	5
F.1. Pascal-Part-116	5
F.2. ADE20K-Part-234	5
F.3. PartImageNet	6
F.4. PartImageNet (OOD)	6

A. Limitations & Future Work

Our PartCATSeg framework has shown strong performance but also has some limitations and potential directions for future work. Specifically, it struggles with handling extremely fine-grained part distinctions, where subtle differences between parts are challenging to capture accurately. Additionally, the framework is designed based on semantic segmentation, as it continues to demonstrate superior performance compared to instance segmentation in many scenarios. However, this design choice inherently limits the ability to distinguish individual parts as separate instances. For example, distinguishing between the left and right handles of a bicycle requires an instance-level understanding that the current framework lacks. Achieving this would necessitate the generation or inclusion of instance object masks, which are not currently supported. Expanding the framework to incorporate instance segmentation could address this limitation, enabling more precise and versatile part segmentation for applications that demand detailed instance-level information.

Future work aims to address these limitations by improving fine-grained differentiation through advanced attention mechanisms [23, 47, 68] and adaptive structural priors tailored to specific datasets. Enhancing the framework’s ability to distinguish subtle part-level differences could significantly improve its performance in complex scenarios. Additionally, integrating the framework with off-the-shelf open-vocabulary instance segmentation modules offers a promising solution for overcoming the inability to individual parts as separate instances. This integration could enable the model to assign unique labels to similar parts across different instances, further extending its applicability and effectiveness.

B. Experimental Details

B.1. Code & Reproduction

Details can be found in the publicly available code. For additional details, refer to the anonymized GitHub repository available at <https://github.com/kaist-cvml/part-catseg>

B.2. Device Information

All experiments were conducted using eight NVIDIA A6000 GPUs and PyTorch 2.2 for training and evaluation.

B.3. Implementation Details

Our model is based on CAT-Seg [13], a state-of-the-art open-vocabulary semantic segmentation (OVSS) method, redefined to suit open-vocabulary part segmentation (OVPS) tasks in OV-PARTS [70]. It employs a CLIP [57] encoder built on CLIP ViT-B/16 and leverages DINOv2 [54], a pre-trained model, for structural guidance.

We begin by utilizing the pre-trained object-level OVSS models from CAT-Seg and fine-tune them with the datasets described in Appendix F. The model undergoes training with the AdamW [49] optimizer, starting with an initial learning rate of 0.0001, over 20,000 iterations, and a batch size of 8. During training, model checkpoints are saved every 1,000 iterations. The final model is selected based on the highest validation performance. For instance, the best validation score on the Pascal-Part-116 dataset in the Oracle-Obj setting comes from the checkpoint saved at 12,000 iterations.

B.4. Evaluation Details

For the evaluation protocol, the Pred-All setup of PartCLIPSeg [14] and the Oracle-Obj setup of OV-PARTS [70] were utilized. The Pred-All setup assumes a more challenging scenario in which predictions are made without any prior information. In contrast, the Oracle-Obj setup assumes the availability of object-level masks. As noted in OV-PARTS, the Oracle-Obj setup simulates results achievable when using off-the-shelf open-vocabulary semantic segmentation models.

B.5. Hyperparameters

The model architecture incorporates layers and parameters from CAT-Seg [13]. Furthermore, as outlined in Equation (15), our method defines three key hyperparameters, λ_{obj} , λ_{part} , and λ_{comp} , which are associated with two primary loss functions: the disentanglement loss $\mathcal{L}_{\text{disen}}$ and the compositional loss $\mathcal{L}_{\text{comp}}$. These lambda parameters were fine-tuned through experimental validation on the training set to balance the contributions of the proposed loss functions. The final values were determined as $\lambda_{\text{obj}} = 1.0$, $\lambda_{\text{part}} = 1.0$, and $\lambda_{\text{comp}} = 1.0$.

B.6. Baselines

- ZSSeg+ [70, 74]: ZSSeg is a two-stage framework for open-vocabulary semantic segmentation that uses CLIP to classify class-agnostic mask proposals, enabling segmentation of seen and unseen classes. ZSSeg+ extends ZSSeg to support part-level segmentation. We evaluate ZSSeg+ using a ResNet-50 [27] baseline, fine-tuned with Compositional Prompt Tuning based on CoOp [82].
- VLPART [61]: VLPART enables open-vocabulary part segmentation by training on data across multiple granularities (part-level, object-level, and image-level) and segments novel objects into parts through dense correspondences with base objects.
- CLIPSeg [50, 70]: CLIPSeg extends CLIP for segmentation tasks, using a transformer-based decoder to generate segmentation maps conditioned on text or image prompts, supporting tasks like referring expression segmentation and zero-shot segmentation. For evaluation, we fine-tune the FiLM layer, decoder, visual encoder, and language embedding layer in the text encoder, following the approach in [70].
- CAT-Seg [13, 70]: CAT-Seg adapts vision-language models like CLIP by aggregating cosine similarity between image and text embeddings to create cost volumes, enabling segmentation of seen and unseen classes. Additionally, CAT-Seg proposes learning the self-attention heads of CLIP’s encoders, achieving effective results.

- PartGLEE [38]: PartGLEE is a part-level segmentation model that uses a unified framework and the Q-Former to model hierarchical relationships between objects and parts, allowing segmentation at any granularity in open-world scenarios.
- PartCLIPSeg [14]: PartCLIPSeg leverages generalized parts and object-level contexts to enhance fine-grained part segmentation, incorporating competitive part relationships and attention mechanisms to improve segmentation accuracy and generalization to unseen vocabularies.

C. Additional Quantitative Evaluation

C.1. Evaluation on Recall

We evaluated various baselines across multiple datasets, as detailed in Table 1, Table 2, and Table 3. Here, we provide an additional analysis of recall performance in zero-shot evaluation on Pascal-Part-116 and ADE20K-Part-234. The recall metric measures a model’s ability to correctly identify less frequent or smaller objects, which are often more difficult to segment accurately. As shown in Table A1, our method achieves state-of-the-art recall scores, highlighting its superior capability in identifying and segmenting these challenging parts.

Method	Pascal-Part-116			ADE20K-Part-234		
	Seen	Unseen	h-Recall	Seen	Unseen	h-Recall
ZSSeg+ [74]	<u>65.47</u>	32.13	43.10	<u>55.78</u>	40.71	47.07
CLIPSeg [50, 70]	55.71	43.35	48.76	49.59	48.11	48.84
CAT-Seg [13, 70]	56.00	43.20	48.77	43.48	39.87	41.60
PartCLIPSeg [14]	58.46	<u>47.93</u>	<u>52.67</u>	53.31	<u>51.52</u>	<u>52.40</u>
PartCATSeg (Ours)	67.15	61.02	63.94	64.81	64.22	64.52

¹ The best score is **bold** and the second-best score is underlined.

Table A1. Comparison of zero-shot performance with state-of-the-art methods in terms of **Recall** for **Oracle-Obj** setting on Pascal-Part-116.

C.2. DINO Structural Guidance

We confirmed the effectiveness of DINO’s structural guidance for PartCATSeg in Table 6 of the main text. Additionally, the supplementary material examines how DINO’s structural guidance impacts the original CAT-Seg. As shown in Table A2, while DINO’s structural guidance proves effective, its performance improvement is relatively modest compared to the proposed PartCATSeg. This highlights that the proposed framework for disentangling parts is more effective overall.

Method	Pred-All			Oracle-Obj		
	Seen	Unseen	h-IoU	Seen	Unseen	h-IoU
CAT-Seg	36.80	23.39	28.60	43.81	27.66	33.91
CAT-Seg w/ Structural Guidance	38.84	28.99	33.20	50.37	36.86	42.57
PartCATSeg w/o Structural Guidance	42.29	27.94	33.65	46.44	31.59	37.60
PartCATSeg	52.62	40.51	45.77	57.49	44.88	50.41

¹ The best score is **bold**.

Table A2. Comparison of zero-shot performance with state-of-the-art methods on Pascal-Part-116.

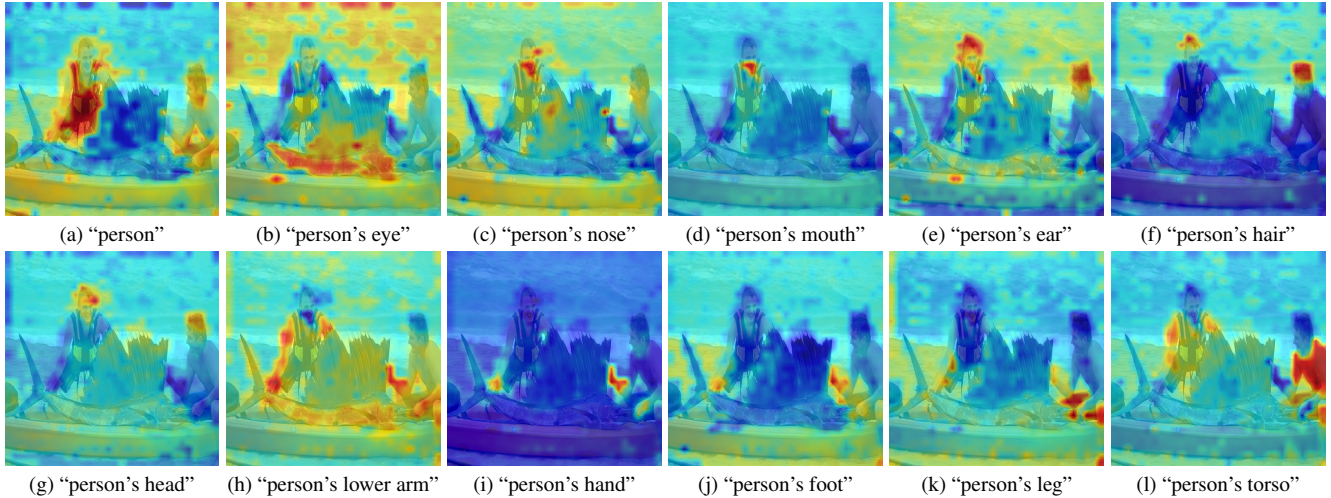


Figure A1. Image-Text Correspondence Visualization **Before** Training

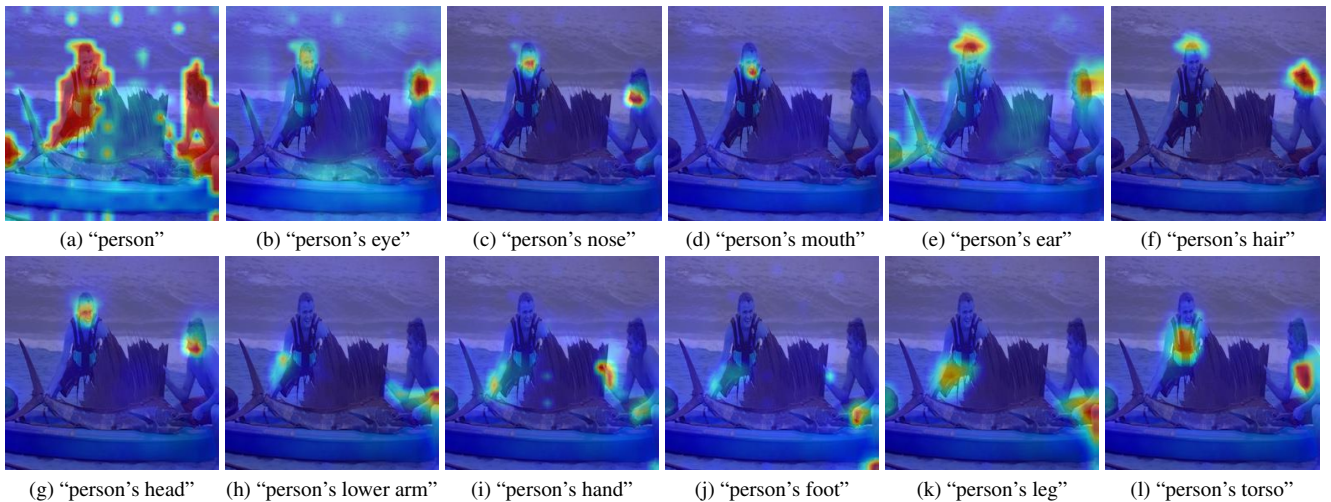


Figure A2. Image-Text Correspondence Visualization **After** Training

D. Additional Qualitative Results

D.1. Pascal-Part-116 (Oracle-Obj Setting)

The Figure A8 illustrates qualitative evaluations under the Oracle-Obj setting, which assumes that object masks are provided. This setting evaluates the fine-grained part segmentation results using object-level segmentation generated by other off-the-shelf OVSS models.

PartCATSeg consistently demonstrates superior segmentation performance compared to other baselines. Notably, it effectively segments small parts, such as arms and eyes, which are often missed by other models.

D.2. PartImageNet (Pred-All Setting)

The following Figure A9 illustrates the PartImageNet prediction results of PartCATSeg in Pred-All setup. PartCATSeg demonstrates superior performance compared to other baselines, accu-

rately predicting both appropriate classes and boundaries.

D.3. PartImageNet (Oracle-Obj Setting)

The following Figure A10 illustrates the PartImageNet prediction results of PartCATSeg in Oracle-Obj setup. PartCATSeg demonstrates superior performance compared to other baselines, accurately predicting appropriate boundaries.

D.4. Cost Visualization

The following Figure A2 and Figure A4 present the cost (correspondence) visualization after training. It visualizes the object-specific part correspondence between the caption text and the image. Unlike (pretrained) CLIP Image-Text Similarity Visualization (Figure 2) discussed in Section 1 and Figure A1, as well as Figure A3, the cost volume demonstrates significant improvement in fine-grained alignment after training, as illustrated in Figure A2 and Figure A4.

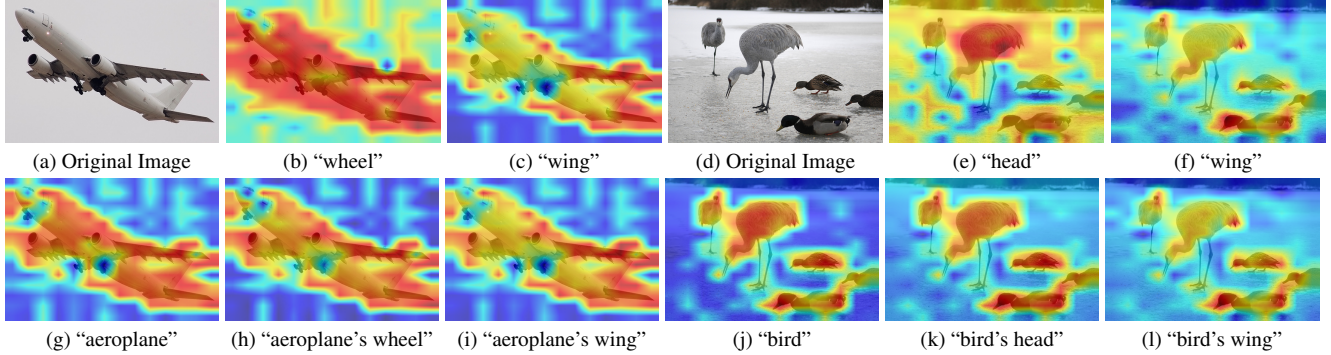


Figure A3. **CLIP Image-Text Similarity Visualization for Object-Level and Part-Level Text.** The visualization compares the frozen CLIP image-text similarity between object-level and part-level text descriptions. (a), (d) show the original images; (b), (c), (e), (f) depict the part-level similarities for terms such as "wheel" and "wing" while (g)-(l) show object-specific parts. The stronger activation for object-level text suggests a dominant focus on the entire object rather than individual parts in the image-text correspondence.

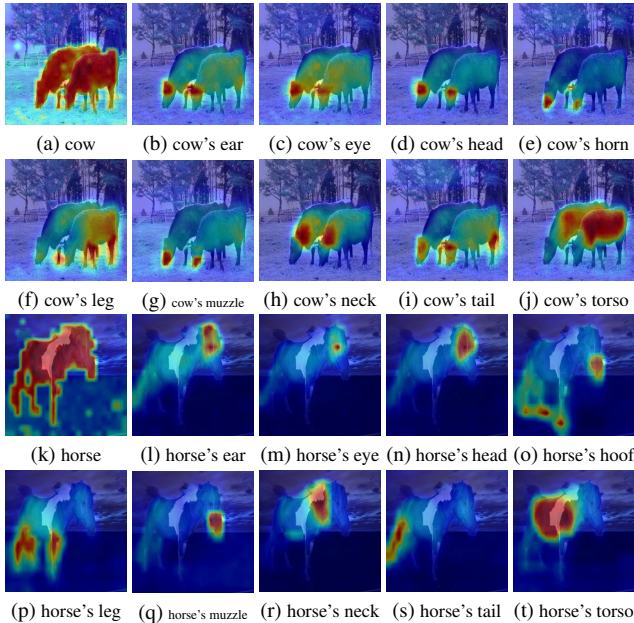


Figure A4. **Cost Volume Visualization After Additional Training.** Cost volume visualization showed that PartCATSeg significantly enhanced fine-grained alignment.

E. Additional Ablation Study

E.1. Compositional Loss

As detailed in Section 3.5, parts are not only compositional components that constitute an object but also maintain relationships with adjacent parts. Previous methodologies have proposed learning strategies that consider granularity at two levels—the object and its parts. However, they have not focused on the composition of object-specific parts within the object and the relationships between these parts. This limitation often results in small parts, such as "cat's eye" and "cat's neck", being undetected within the context of a larger object, as shown in Figure A5a. We hypoth-

esize that this issue arises because certain parts become excessively dominant relative to other parts they encompass, leading to a failure to recognize their spatial and compositional relationships. By introducing compositional loss, our model better identifies and segments smaller or more discriminative parts. As illustrated in Figure A5, the inclusion of compositional loss resolves issues of overlapping or diffuse cost volumes, as visualized in Figure A5c and Figure A5d. These visualizations highlight how compositional loss sharpens the focus on specific parts, mitigating the spread of cost volume and ensuring better part-level segmentation.

Furthermore, as shown in Figure A6, compositional loss consistently improves segmentation performance across datasets. For example, in Pascal-Part-116, it enhances the segmentation of challenging parts such as "cow's eye" or "cat's nose," which are often difficult to detect. Specifically, the comparison demonstrates that softmax normalization in the compositional loss ($\mathcal{L}_{\text{comp-SM}}$) outperforms L1 normalization ($\mathcal{L}_{\text{comp-L1}}$). Similarly, as shown in Figure A7, compositional loss demonstrates its effectiveness in capturing fine-grained part relationships in PartImageNet, such as "goose's tail," "tench's tail," and "killer whale's head." This improvement underscores the importance of explicitly modeling compositional relationships in part segmentation, particularly for smaller or less distinct parts.

The effectiveness of compositional loss is further validated through quantitative results, as shown in Table A3. The inclusion of $\mathcal{L}_{\text{comp}}$ improves performance across both the Pred-All and Oracle-Obj settings on PartImageNet. Notably, it enhances the harmonic IoU for unseen parts, demonstrating its ability to better capture fine-grained compositional relationships and improve segmentation consistency for challenging parts.

Compositional Loss	Pred-All			Oracle-Obj		
	Seen	Unseen	h-IoU	Seen	Unseen	h-IoU
w/o $\mathcal{L}_{\text{comp}}$	59.21	50.75	54.66	72.17	68.42	70.24
w/ $\mathcal{L}_{\text{comp}}$	57.33	53.07	55.12	73.83	71.52	72.66

Table A3. Impact of Compositional Loss on PartImageNet

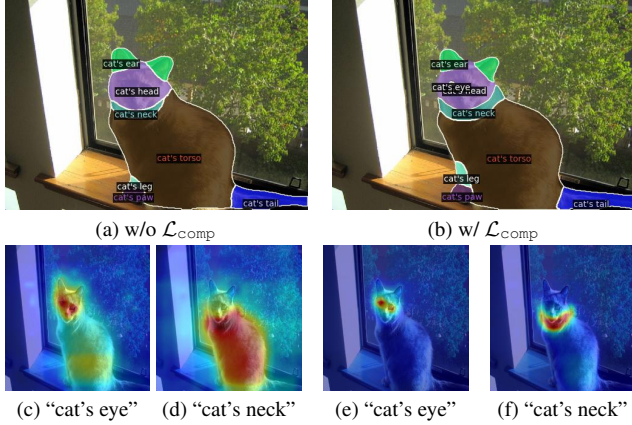


Figure A5. **Ablation on Compositional Loss.** (a) and (b) show segmentation results without and with $\mathcal{L}_{\text{comp}}$, respectively. (c) and (d) show less defined cost volumes without $\mathcal{L}_{\text{comp}}$, while (e) and (f) reveal more exclusive similarities in the cost volumes with $\mathcal{L}_{\text{comp}}$. Notably, "cat's eye" is successfully segmented with the inclusion of $\mathcal{L}_{\text{comp}}$.

F. Datasets Details

F.1. Pascal-Part-116

Pascal-Part-116 [70] is a modified version of the Pascal-Part [8] dataset specifically designed for Open-Vocabulary Part Segmentation tasks. The dataset includes a mix of base and novel categories, focusing on diverse object-level classes. It features novel classes for the object categories "bird", "car", "dog", "sheep", and "motorbike". Additionally, based on object-specific part categories, the dataset comprises 74 base categories and 42 novel categories, offering a comprehensive benchmark for evaluating segmentation models. Detailed information about the base and novel classes can be found in Table A4.

Pascal-Part-116 Object-specific Part Categories				
Base Categories (74)				
aeroplane's body	aeroplane's stern	aeroplane's wing	aeroplane's tail	aeroplane's engine
aeroplane's wheel	bicycle's wheel	bicycle's saddle	bicycle's handlebar	bicycle's chainwheel
bicycle's headlight	bottle's body	bottle's cap	bus's wheel	bus's headlight
bus's front	bus's side	bus's back	bus's roof	bus's mirror
bus's license plate	bus's door	bus's window	cat's tail	cat's head
cat's eye	cat's torso	cat's neck	cat's leg	cat's nose
cat's paw	cat's ear	cow's tail	cow's head	cow's eye
cow's torso	cow's neck	cow's leg	cow's ear	cow's muzzle
cow's horn	horse's tail	horse's head	horse's eye	horse's torso
horse's neck	horse's leg	horse's ear	horse's muzzle	horse's hoof
person's head	person's eye	person's torso	person's neck	person's leg
person's foot	person's nose	person's ear	person's eyebrow	person's mouth
person's hair	person's lower arm	person's upper arm	person's hand	pottedplant's pot
pottedplant's plant	train's headlight	train's head	train's front	train's side
train's back	train's roof	train's coach	tvmonitor's screen	
Novel Categories (42)				
bird's wing	bird's tail	bird's head	bird's eye	bird's beak
bird's torso	bird's neck	bird's leg	bird's foot	bird's wheel
car's headlight	car's front	car's side	car's back	car's roof
car's mirror	car's license plate	car's door	car's window	dog's tail
dog's head	dog's eye	dog's torso	dog's neck	dog's leg
dog's nose	dog's paw	dog's ear	dog's muzzle	motorbike's wheel
motorbike's saddle	motorbike's handlebar	motorbike's headlight	sheep's tail	sheep's head
sheep's eye	sheep's torso	sheep's neck	sheep's leg	sheep's ear
sheep's muzzle	sheep's horn			

Table A4. List of object-specific classes in **Pascal-Part-116**.

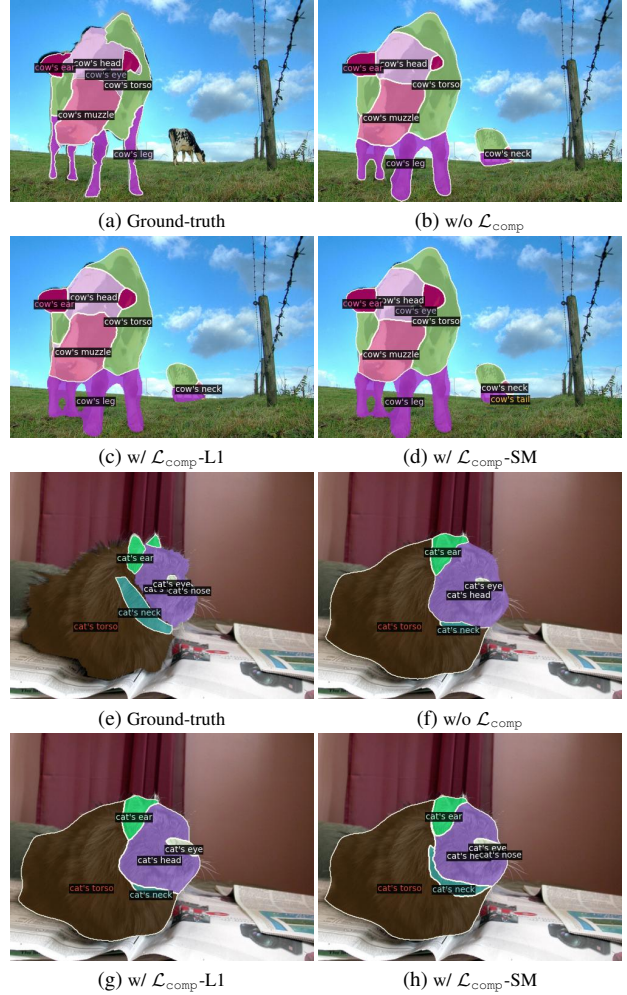
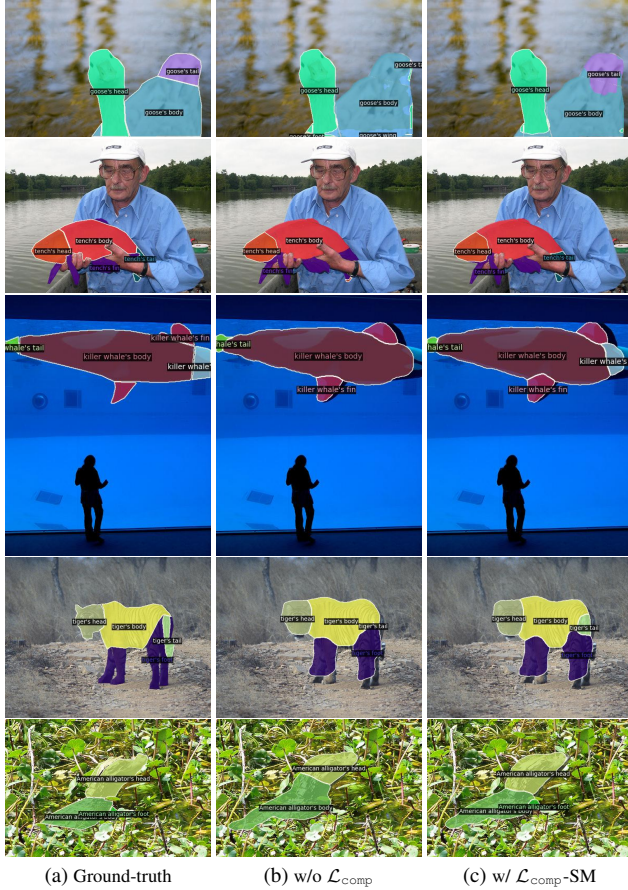


Figure A6. **Qualitative Ablation on Compositional Loss for Pred-All setting in Pascal-Part-116.** Applying compositional loss improves segmentation performance, particularly for challenging parts like "cow's eye" or "cat's nose". Furthermore, using softmax normalization in the compositional loss ($\mathcal{L}_{\text{comp-SM}}$) outperforms L1 normalization ($\mathcal{L}_{\text{comp-L1}}$) by better capturing these fine-grained parts such as "cat's neck".

F.2. ADE20K-Part-234

ADE20K-Part-234 [70] is an adapted version of the ADE20K dataset [80] tailored for Open-Vocabulary Part Segmentation tasks. The dataset includes a mix of base and novel categories, with a focus on a diverse range of object-level classes. It features novel classes for the object categories "bench", "bus", "fan", "desk", "stool", "truck", "van", "swivel chair", "oven", "ottoman," and "kitchen island". Additionally, based on object-specific part categories, the dataset comprises 176 base categories and 58 novel categories, providing a robust benchmark for evaluating segmentation models. The dataset presents additional challenges due to its diverse categories and the frequent appearance of small parts, which require precise part segmentation.



(a) Ground-truth (b) w/o \mathcal{L}_{comp} (c) w/ $\mathcal{L}_{comp} + SM$

Figure A7. **Qualitative Ablation on Compositional Loss in PartImageNet.** The first two rows show results in the Oracle-Obj setting, while the bottom three rows are in the Pred-All setting. Segmentation with \mathcal{L}_{comp} captures finer part relationships, such as “goose’s tail,” “tench’s tail,” “killer whale’s head,” “tiger’s tail,” and “American alligator’s foot,” compared to results without \mathcal{L}_{comp} .

F.3. PartImageNet

PartImageNet [25] is a dataset adapted from ImageNet [17], comprising approximately 24,000 images across 158 categories, each annotated with detailed part information. These categories are grouped into 11 superclasses, based on the hierarchical taxonomy provided by WordNet [51]. In cross-dataset evaluation settings, PartImageNet categories are not pre-divided into base and novel classes. Therefore, for zero-shot evaluation, we select 40 representative object classes from the dataset, which we further split into 25 base object classes and 15 novel object classes, just as in PartCLIPSeg [14]. Each superclass contains corresponding part classes, allowing us to construct part categories by associating these object classes with their respective part classes within each superclass. This selective splitting ensures that the novel classes remain unseen during training, thereby providing a robust evaluation of zero-shot capabilities. Detailed information about the base and novel classes, along with their corresponding superclasses, is presented in Table A6.

ADE20K-Part-234 Object-specific Part Categories

Base Categories (176)				
person's arm	person's back	person's foot	person's gaze	person's hand
person's head	person's leg	person's neck	person's torso	door's door frame
door's handle	door's knob	door's panel	clock's face	clock's frame
toilet's bowl	toilet's cistern	toilet's lid	cabinet's door	cabinet's drawer
cabinet's front	cabinet's shelf	cabinet's side	cabinet's skirt	cabinet's top
sink's bowl	sink's faucet	sink's pedestal	sink's tap	sink's tap
lamp's arm	lamp's base	lamp's canopy	lamp's column	lamp's cord
lamp's highlight	lamp's light source	lamp's shade	lamp's tube	score's arm
score's backplate	score's highlight	score's light source	score's shade	chair's apron
chair's arm	chair's back	chair's base	chair's leg	chair's seat
chair's seat cushion	chair's skirt	chair's stretcher	chest of drawers's apron	chest of drawers's door
chest of drawers's drawer	chest of drawers's front	chest of drawers's leg	chandelier's arm	chandelier's bulb
chandelier's canopy	chandelier's chain	chandelier's cord	chandelier's highlight	chandelier's light source
bed's headboard	bed's footboard	table's leg	bed's leg	bed's side rail
table's apron	table's wheel	table's shelf	table's shelf	table's top
armchair's arm	armchair's apron	armchair's seat base	armchair's back	armchair's back pillow
armchair's leg	armchair's seat	sofa's arm	armchair's seat cushion	sofa's leg
sofa's arm	sofa's back	sofa's skirt	sofa's leg	coffee table's top
sofa's seat cushion	sofa's skirt	wardrobe's door	wardrobe's front	wardrobe's leg
computer's mouse	wardrobe's mirror	wardrobe's top	wardrobe's drawer	wardrobe's leg
wardrobe's mirror	car's hood	car's license plate	car's bumper	car's headlight
car's hood	car's window	car's wiper	car's logo	car's mirror
car's window	cooking stove's burner	cooking stove's oven	cooking stove's stove	cooking stove's button panel
cooking stove's drawer	cooking stove's oven	refrigerator's door	refrigerator's side	refrigerator's button panel
refrigerator's door	refrigerator's side	dishwasher's drawer	dishwasher's top	dishwasher's handle
dishwasher's skirt	television receiver's base	television receiver's buttons	television receiver's frame	television receiver's screen
television receiver's base	television receiver's speaker	pool table's leg	pool table's pocket	airplane's fuselage
pool table's leg	airplane's propeller	minibike's license plate	minibike's seat	minibike's wheel
minibike's license plate	minibike's mirror	washer's door	washer's front	washer's pole
light's aperture	light's canopy	light's diffuser	light's housing	light's light source
light's shade				
Novel Categories (58)				
ottoman's back	ottoman's leg	ottoman's seat	swivel chair's back	swivel chair's base
swivel chair's seat	swivel chair's wheel	fan's blade	fan's canopy	fan's tube
stool's leg	stool's seat	desk's apron	desk's door	desk's drawer
desk's leg	desk's shelf	desk's top	bus's bumper	bus's door
bus's headlight	bus's license plate	bus's logo	bus's mirror	bus's wheel
bus's window	bus's wiper	oven's button panel	oven's door	oven's drawer
oven's top	kitchen island's door	kitchen island's drawer	kitchen island's front	kitchen island's side
kitchen island's top	van's bumper	van's door	van's headlight	van's license plate
van's logo	van's mirror	van's taillight	van's wheel	van's window
van's wiper	truck's bumper	truck's door	truck's headlight	truck's license plate
truck's logo	truck's mirror	truck's wheel	truck's window	bench's arm
bench's back	bench's leg			

Table A5. List of object-specific classes in ADE20K-Part-234.

Superclass	Base Object Categories (25)	Novel Object Categories (15)	Part Classes
Quadruped	tiger, giant panda, leopard, gazelle	ice bear, impala, golden retriever	Head, Body, Foot, Tail
Snake	green mamba	Indian cobra	Head, Body
Reptile	green lizard, Komodo dragon, tree frog	box turtle, American alligator	Head, Body, Foot, Tail
Boat	yawl, pirate	schooner	Body, Sail
Fish	barracouta, goldfish, killer whale	tench	Head, Body, Fin, Tail
Bird	albatross, goose	bald eagle	Head, Body, Wing, Foot, Tail
Car	garbage truck, minibus, ambulance	jeep, school bus	Body, Tier, Side Mirror
Bicycle	mountain bike, moped	motor scooter	Body, Head, Seat, Tier
Biped	gorilla, orangutan	chimpanzee	Head, Body, Hand, Foot, Tail
Bottle	beer bottle, water bottle	wine bottle	Mouth, Body
Aeroplane	warplane	airliner	Head, Body, Engine, Wing, Tail

Table A6. List of selected object classes and their corresponding part classes per superclass from PartImageNet [25]. Object categories are categorized into base and novel object classes, with part classes assigned to each respective superclass.

F.4. PartImageNet (OOD)

PartImageNet [25] offers an alternative split designed for few-shot learning, which ensures non-overlapping classes across the training and validation sets. This few-shot split includes 109 base object classes in the training set and 19 novel object classes in the validation set. Detailed information about the base and novel classes, along with their corresponding superclasses, is presented in Table A7.

Superclass	Base Object Categories (109)	Novel Object Categories (19)
Quadruped	impala, Egyptian cat, warthog, otter, Tibetan terrier timber wolf, polecat, water buffalo, ox, redbone English springer, tiger, American black bear, leopard, hartebeest vizsla, Brittany spaniel, giant panda, Boston bull, ram cairn, Arabian camel, fox squirrel, Eskimo dog, Irish water spaniel Saluki, Walker hound, cheetah, gazelle, soft-coated wheaten terrier bighorn, brown bear, chow, weasel	golden retriever, cougar, ice bear, mink, Saint Bernard
Snake	night snake, boa constrictor, green mamba, thunder snake, green snake hognose snake, sidewinder, horned viper, diamondback, rock python garter snake, vine snake	Indian cobra
Reptile	Gila monster, common newt, green lizard, bullfrog, American alligator leatherback turtle, spotted salamander, box turtle, tailed frog, African chameleon Komodo dragon, agama, frilled lizard, loggerhead	whiptail, alligator lizard
Boat	yawl, pirate	trimaran
Fish	goldfish, coho, tench, anemone fish, killer whale	barracouta, great white shark
Bird	albatross, spoonbill, black stork, dowitcher, American egret goose, ruddy turnstone, bee eater, kite	little blue heron, bald eagle
Car	garbage truck, minibus, ambulance, snowplow, golfcart police van, minivan, convertible, limousine, recreational vehicle go-kart, tractor, school bus, racer	beach wagon, cab
Bicycle	motor scooter, tricycle, mountain bike	unicycle
Biped	gorilla, gibbon, guenon, macaque, patas howler monkey, chimpanzee, proboscis monkey, spider monkey, baboon colobus, capuchin	siamang, marmoset
Bottle	beer bottle, pop bottle, pill bottle	water bottle
Aeroplane	airliner	

Table A7. **PartImageNet (OOD)**. List of selected object classes and their corresponding part classes per superclass from PartImageNet (OOD) [25]. Object categories are divided into base and novel object classes. Detailed associations of part classes with their respective superclasses are provided in Table A6.

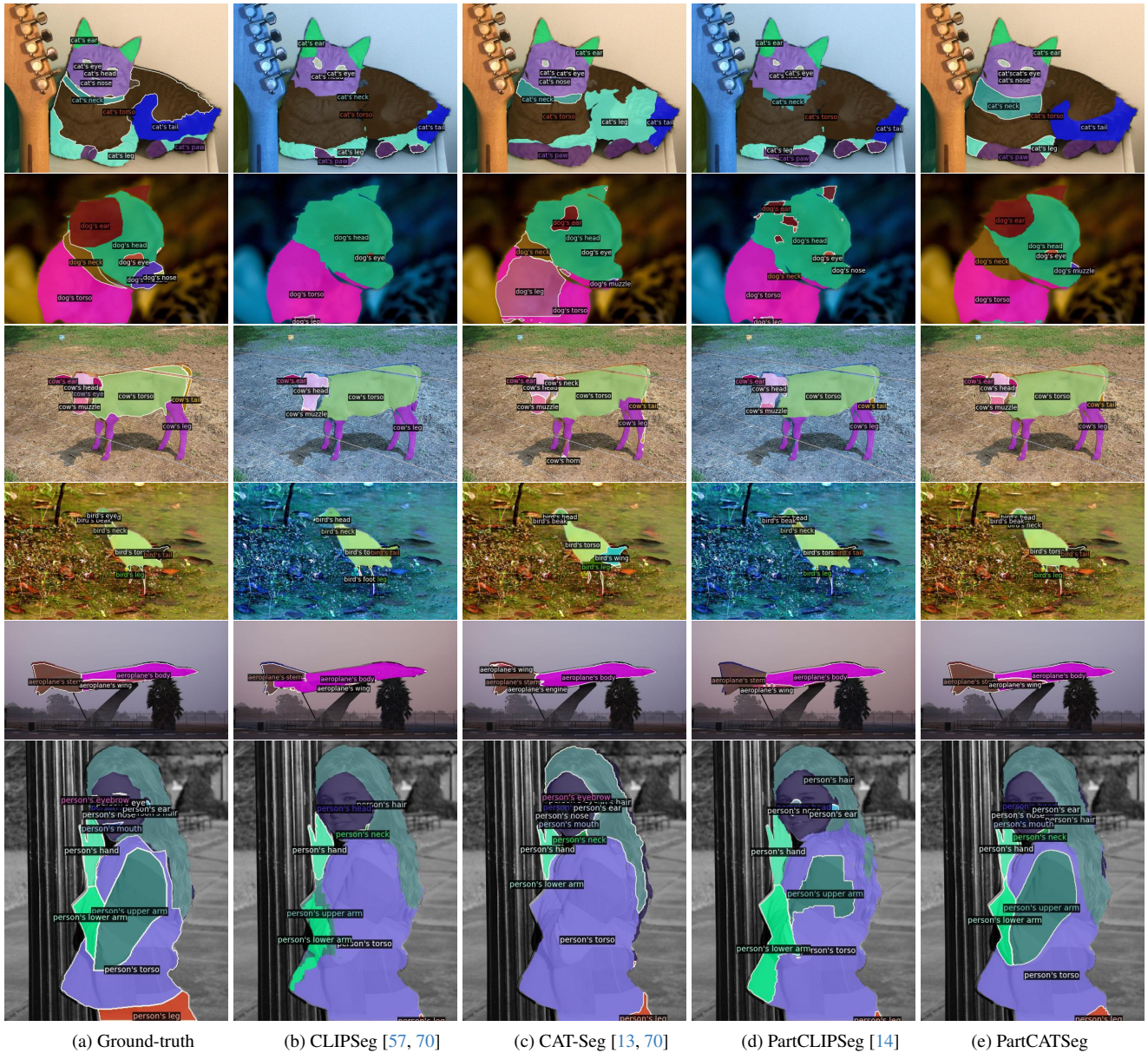
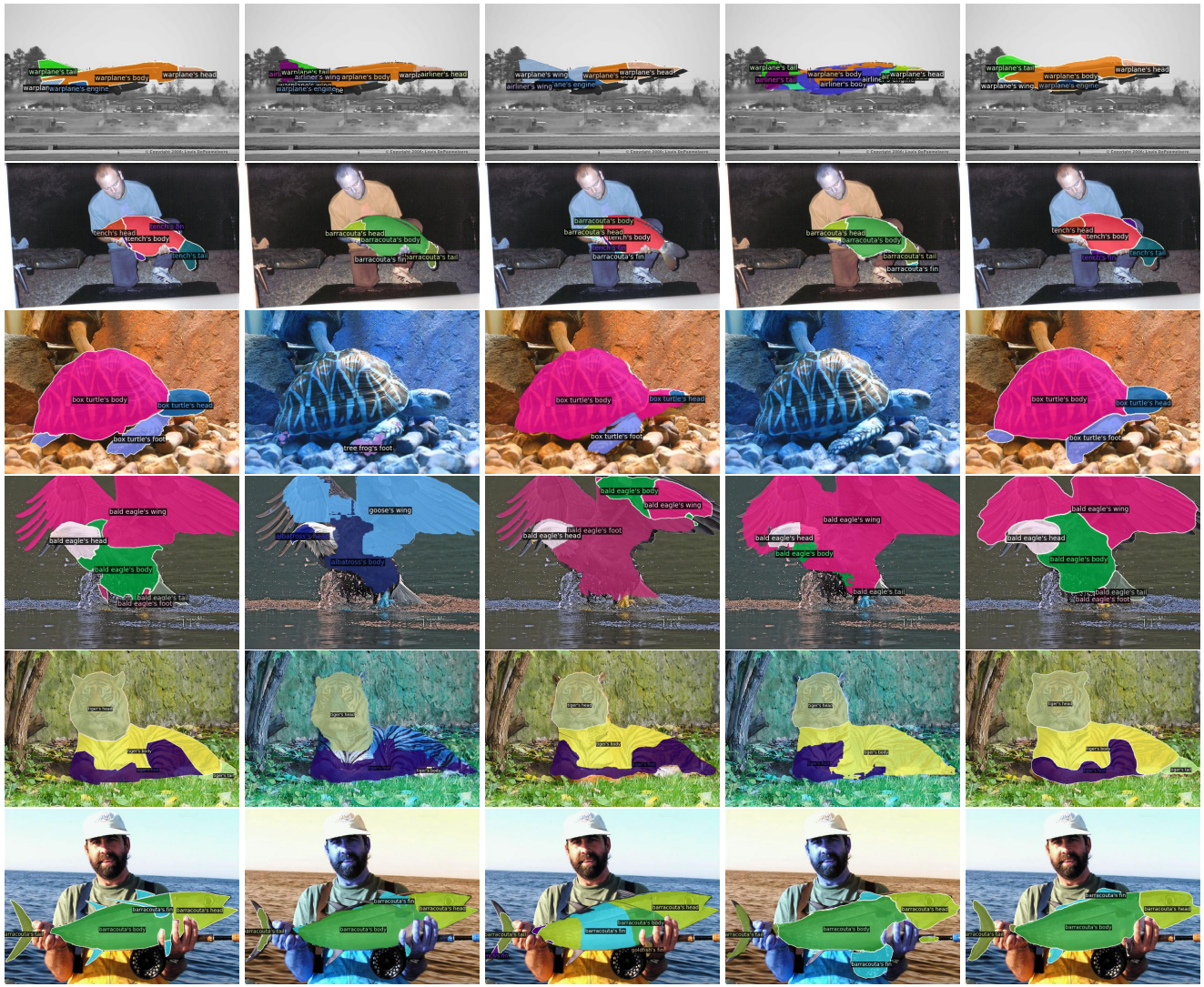


Figure A8. Qualitative evaluation of zero-shot part segmentation on Pascal-Part-116 in the **Oracle-Obj** configuration. Note that annotations for unseen categories (e.g., bird, cow, dog) are excluded from the training set.



(a) Ground-truth

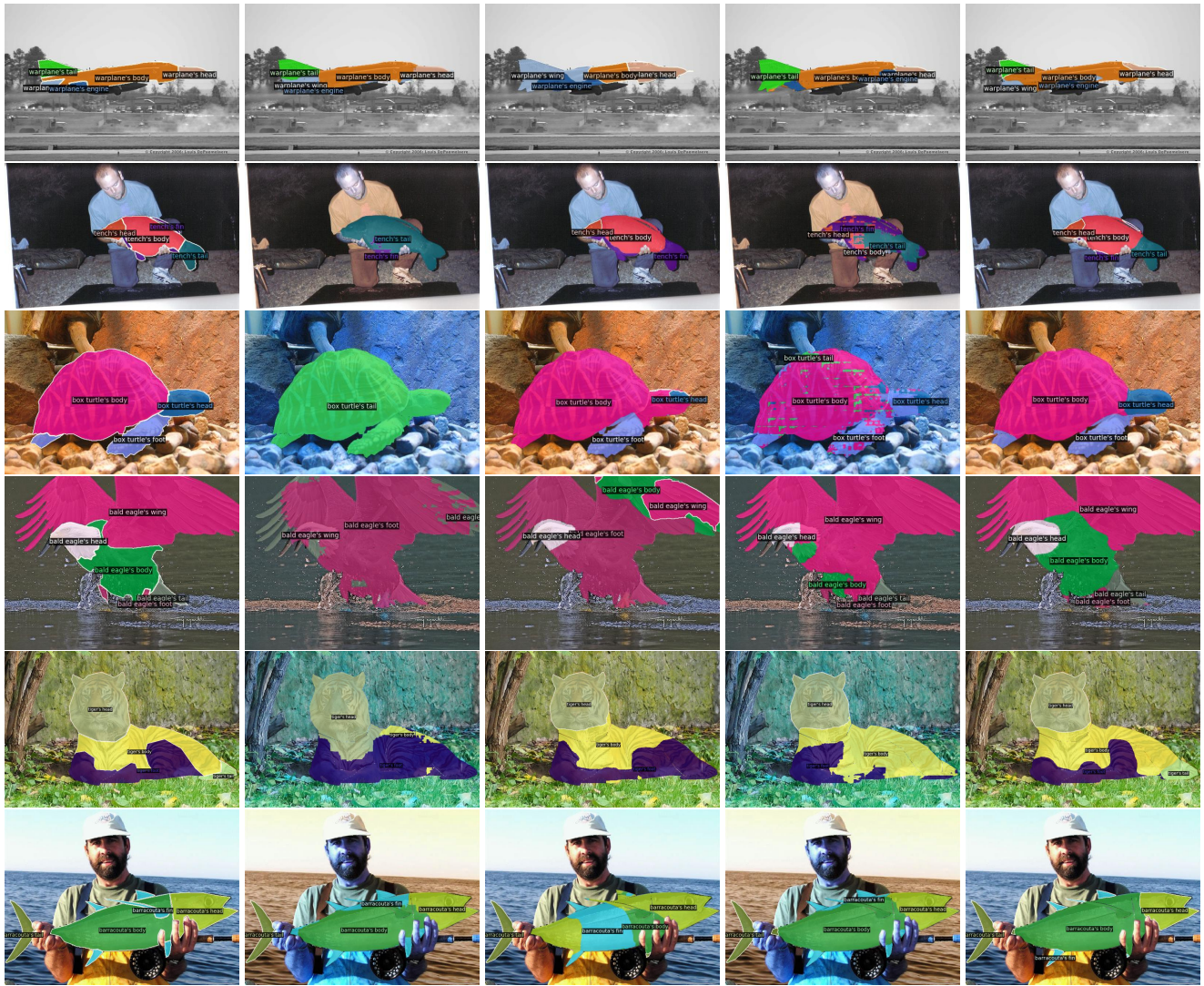
(b) CLIPSeg [57, 70]

(c) CAT-Seg [13, 70]

(d) PartCLIPSeg [14]

(e) PartCATSeg

Figure A9. Qualitative evaluation of zero-shot part segmentation on **PartImageNet** in the **Pred-All** configuration.



(a) Ground-truth

(b) CLIPSeg [57, 70]

(c) CAT-Seg [13, 70]

(d) PartCLIPSeg [14]

(e) PartCATSeg

Figure A10. Qualitative evaluation of zero-shot part segmentation on PartImageNet in the **Oracle-Obj** configuration.